2022

A computational fluid dynamic, experimental and empirical analysis of University of Plymouth's Brunel laboratories shell and tube heat exchanger

Hill, L.

Hill, L. (2022) 'A computational fluid dynamic, experimental and empirical analysis of University of Plymouth's Brunel laboratories shell and tube heat exchanger', The Plymouth Student Scientist, 15(1), pp. 69-103.
http://hdl.handle.net/10026.1/19457

The Plymouth Student Scientist
University of Plymouth

*The Plymouth Student Scientist, 2022, **15**, (1), 69-103*

A computational fluid dynamic, experimental and empirical analysis of University of Plymouth's Brunel laboratories shell and tube heat exchanger

Luke Hill

Project Advisor: Adam Kyte, School of Engineering, Computing and Mathematics, University of Plymouth, Drake Circus, Plymouth, PL4 8AA

Abstract

The aim of this paper is to analyse the University of Plymouth's Brunel laboratories shell and tube heat exchanger using three investigative methods aiming to determine which method most accurately predicts the heat exchanger performance. The university heat exchanger, UHX, uses the TECQUIPMENT TD360C shell and tube heat exchanger but an experimental study could not be conducted so data was collated from previous experiments. This was used to calculate an experimental value for the overall heat transfer coefficient (U). Two empirical methods were used, the Kern and Bell-Delaware method. These two methods were developed in the mid to late 20th century to provide a prediction for U without having to conduct an experimental analysis. Finally, a computational fluid dynamic (CFD), study was performed using ANSYS CFX CFD package.

To validate the accuracy of the CFD model a study by Ozden and Tari (2010) was used. As their method was unclear CFD best practices were used. The major differences were changing the turbulence model from the k-ϵ to the SST model, increasing the mesh resolution in the boundary layers and conducting a transient analysis.

It was concluded that the validation case CFD was not accurate, and the actual performance was 108-150% greater than theirs. For the UHX, the Kern and Bell-Delaware methods underpredicted the averaged experimental values by 73-76% and 46-77% Consequently, these methods were deemed insufficient for the prediction of heat exchanger performance. Compared to the validation case the CFD method was changed for the UHX with the modelling of the tubes and tubes volume. It was found that the parallel-flow and counter-flow CFD results overpredicted the experimental results by 16-30% and 18-36%. As the CFD method did not include any real-world problems such as baffle leakage and fluctuations in inlet temperature it was deemed to be the most accurate method for predicting heat exchanger performance.

Keywords: Shell and tube heat exchanger, CFD, ANSYS CFX, Kern method, Bell-Delaware method

Introduction

Shell and tube heat exchangers are a through-the-wall heat exchanger where a bundle of tubes is contained within a cylindrical shell. Fluids at different temperatures flow within the shell and the tubes creating a thermal gradient resulting in heat transfer. Heat exchangers have many industrial applications such as preheating of crude oil before the distillation process (Master, Chunangad & Pushpanathan, 2003). There is also naturally occurring heat exchangers in grey whale flippers and flukes. Here, warm arteries are surrounded by cold veins reducing the artery temperature. When this cooler artery enters the poorly insulated fluke less heat is lost to the environment (Schmidt-Nielsen, 1997).

Due to the wide range of industrial applications assessing the performance of heat exchangers is important. Computational fluid mechanics (CFD) can be used to replicate the fluid flow virtually. In this paper an experimental, two empirical and a CFD study will be carried out on University of Plymouth heat exchanger (UHX). Each of these three methods will be assessed with the overall aim to gain the same result from each analysis. However, if this is not the case then each analytical method will be evaluated to determine which is the most suitable for predicting heat exchanger performance.

Before conducting the three analyses on the UHX the CFD model will be validated by replicating the CFD model developed by Ozden & Tari, 2010. Once validated the model will be applied to the UHX with the results compared against the experimental data and two empirical analyses the Kern and Bell-Delaware methods.

Literature review

Heat Exchanger Theory

Thermodynamics

The fundamentals of heat transfer effect the behaviour of a heat exchanger. Conduction and convection are applicable with radiation only becoming relevant in space applications (Holman, 2010). Conduction arises when heat is transferred from an area of high temperature to an area of low temperature. The rate of heat transfer is dependent on the properties of the material and the magnitude of the temperature difference (Levenspiel, 1984). Heat transfer caused by convection occurs when a temperature difference exists between a solid body and a fluid in motion (Rogers, 1992).

Baffles

Baffle arrangement is considered one of the most effective methods of enhancing heat exchanger performance (Eryener, 2006). Both heat exchangers being modelled use the segmented baffle arrangement. Other types such as helical and trefoil-hole baffles can be utilised for improved heat transfer and pressure drop performance (El Maakoul *et al.*, 2016).

Segmented baffles increase heat transfer by guiding the flow back and forth across the tube bundle in a sinusoidal flow pattern (Figure 1) (Taborek & Spalding, 1983).

Secondly, they act as a support for the tube bundle protecting against deformation and vibrations.

Wang *et al.* (2009) describe several weaknesses when using segmented baffles:

- High shell-side pressure drop caused by contraction and expansion of the shell-side flow
- Low heat transfer efficiency due to “dead zones” located behind the baffles (Figure 1)
- Decreased flow across the tube bundle due to leakage paths

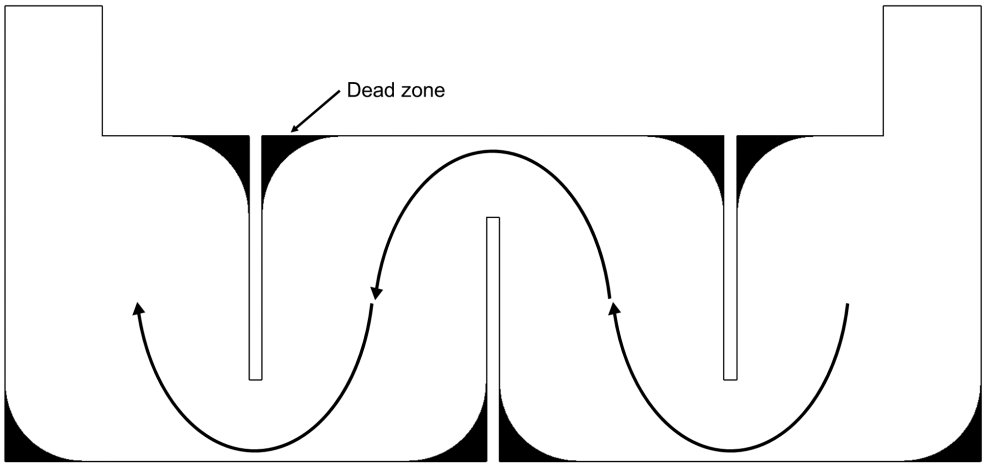

Figure 1: Sinusoidal flow pattern of a segmented baffle heat exchanger with dead zones labelled

Overall Heat Transfer Coefficient

The overall heat transfer coefficient, U, is defined by Equation 1 and can be described as the inverse of the overall resistance to heat flow through a series of thermal mediums. This equation quantifies the thermal resistance per heat transfer area allowing a comparison between different heat exchanger sizes to occur.

U will be used to analyse the heat exchanger performance and compare between the three analytical methods. In other situations where the temperature profile is unknown the ε-NTU method can be used. NTU is a nondimensionalised expression for “heat exchanger size” (Kays & London, 1998).

To determine U the rate of heat transfer, heat transfer area and the log mean temperature difference (LMTD) need to be determined. Rate of heat transfer can be calculated using Equation 2. The temperature difference is the change in the bulk temperature between the inlet and outlet. For the UHX external losses meant that the heat transfer was not equal for the shell and tube side flow and thus an averaged value was used. The heat transfer area is determined based on the geometric dimensions of the heat exchanger. Due to the varying temperature differential between the two fluids the LMTD was used to quantify the average difference in the temperature and is defined by Equation 3.

Equation 1
(Holman, 2010)

$$U = \frac{\dot{Q}}{A\Delta T_{ln}}$$

Where:

$\dot{Q}$ – Rate of heat transfer (W)
U – Overall heat transfer coefficient ($Wm^{-2}K^{-1}$)
A – Heat transfer area (m^2)
ΔT_{ln} – Log mean temperature difference (K)

Equation 2
(Rogers, 1992)

$$\dot{Q} = \dot{m}C_p\Delta T$$

Where:

$\dot{Q}$ – Rate of heat transfer (W)
$\dot{m}$ – Mass flow rate (kgs^{-1})
C_p – Specific heat capacity at constant pressure ($Jkg^{-1}K^{-1}$)
ΔT – Temperature difference (K)

Equation 3
(Rogers, 1992)

$$\Delta T_{ln} = \frac{\Delta T_o - \Delta T_i}{\ln\left(\frac{\Delta T_o}{\Delta T_i}\right)}$$

Where:

ΔT_{ln} – Log mean temperature difference (K)
ΔT_o – Temperature difference outlet (K)
ΔT_i – Temperature difference inlet (K)

The UHX operates two configurations known as parallel-flow and counter-flow. Figure 2 illustrates these configurations on a double pipe heat exchanger where the flow direction changes depending on the configuration. The UHX can operate both configurations where the hot fluid flows through the tubes and cold fluid through the shell. Equation 4 and Equation 5 defines LMTD for the parallel-flow and counter-flow configurations.

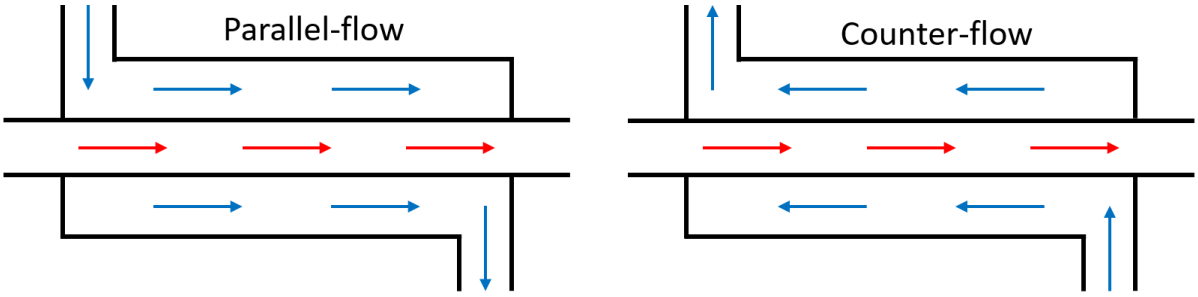

Figure 2: Heat exchanger configurations illustrated on a double pipe heat exchanger

Equation 4
(Rogers, 1992)

Parallel-flow

$$\Delta T_{ln\_p} = \frac{(T_{t2} - T_{s2}) - (T_{t1} - T_{s1})}{\ln\left(\frac{T_{t2} - T_{s2}}{T_{t1} - T_{s1}}\right)}$$

Equation 5 (Rogers, 1992) Counter-flow

$$\Delta T_{\ln\_c} = \frac{(T_{t2} - T_{s1}) - (T_{t1} - T_{s2})}{\ln\left(\frac{T_{t2} - T_{s1}}{T_{t1} - T_{s2}}\right)}$$

Where:

ΔT_{ln} – Log mean temperature difference (K)

T_{s1} – Shell inlet temperature (K) T_{c2} – Shell outlet temperature (K)

T_{h1} – Tube inlet temperature (K) T_{h2} – Tube outlet temperature (K)

Computational Fluid Dynamics

Computational fluid dynamics (CFD) allows the simulation of fluids in motion providing a cost-effective method of simulating real flows (Sayma, 2009). CFD has a wide range of applications including automotive and aerospace engineering (Tu, Yeoh & Liu, 2007). The Navier-stokes continuity equations provide the foundation for modelling a fluid in motion. To account for turbulent flow an average velocity term is introduced into the Navier-stokes equations producing the Reynolds averaged Navier-stokes (RANS) equations. This study will use RANS turbulence models as with a good quality mesh they will provide an accurate solution (Eggenspieler, 2012)

Previous Studies

Researching CFD literature suggested that outside of standard CFD modelling approaches the common trend was using a variation of the k-ε turbulence model. El Maakoul *et al.*, 2016 investigate the heat transfer and pressure drop performance of a variety of baffle arrangements. CFD is used due to the non-conventional baffle designs such as helical and trefoil holed. They use a realizable k-ε turbulence model due to its superior performance for flows involving rotation and boundary layer effects. They correlate their CFD results against an experimental analysis and concluded that their CFD simulation provides adequately accurate results.

Wen *et al*., 2015 also explores the use of non-conventional baffle designs. Their CFD model resembles El Maakoul *et al*. (2016) but they use a renormalization group k-ε turbulence model. They also validated their method against an experimental analysis providing sufficient accuracy.

Ozden and Tari (2010) explore a range of turbulence models and discretization schemes. They conclude that the realizable k-ε turbulence model and first order discretization scheme are the most suitable. Alongside CFD data they also published results for both empirical methods. To decrease the computational demand of the simulation they do not model the tubes and instead use a constant wall temperature of 450K.

This article uses a segmented baffle heat exchanger resembling the UHX. Sufficient information is given to replicate the model but there are some omissions when describing the geometry used. Therefore, this article will be used to validate the CFD model which will then be applied to the UHX. Though this article uses the ANSYS FLUENT CFD package this study will be conducted using ANSYS CFX. All their results are presented in Table 1.

Table 1: Validation case article results (After Ozden and Tari (2010))

Mass flow rate (kgs^{-1})	Empirical methods U ($Wm^{-2}K^{-1}$)		CFD analysis		
	Kern	Bell-Delaware	U ($Wm^{-2}K^{-1}$)	Heat transfer rate (W)	Outlet temp. (K)
0.5	2147	2213	2514	84853	340.40
1.0	3086	3311	3757	131785	330.18
2.0	4489	5025	6768	240506	326.64

Empirical Methods

The Kern and Bell-Delaware methods are commonly used within the literature to empirically assess the performance of heat exchangers. The Kern method was developed in the 1950's and has the simpler calculation method. However, it includes several assumptions impacting its accuracy. Notably the baffle cut is assumed to be always 25% which is not the case for either of the heat exchangers being studied (Donald, 1950). Further, Taborek and Spalding (1983) suggest that the accuracy decreases in the laminar region.

The Bell-Delaware method was developed to provide a more accurate prediction of the overall heat transfer coefficient. Throughout the literature the Bell-Delaware method is the main analytical prediction for heat exchanger performance. This method initially calculates an ideal value which is then adjusted using a series of correction factors. Though both methods can calculate pressure drop only U will be assessed. Taborek and Spalding (1983) present both methods and alongside a simplified online document allowed the relevant calculations to be carried out. Example calculations for the Kern and Bell-Delaware method are presented in appendix A and appendix B.

CFD Validation Case

The study by Ozden and Tari (2010) will be used to verify the CFD method. Their method will not be used exclusively with weaknesses changed for better practices.

Geometry

As the heat exchanger is symmetrical this meant that only half of the model needed to be generated (Figure 3). This allowed a symmetry plain boundary condition to be used significantly reducing the computational demand of the simulation (Tu, Yeoh and Liu, 2007). However, during initial running the location of the outlet was in flow recirculation. This was reducing the accuracy of the results, so the outlet section was extruded a further five times the outlet diameter from the original location (Figure 3).

Only the shell fluid domain was modelled; Baffles, manifolds, shell casing, and other structural components were not. Fillets were introduced at the inlet, outlet and baffle ends to aid the smooth capture of flow around these points. Figure 4 and Figure 5 show the improvement of the mesh at the baffle ends and the inlet. Appendix C

presents the dimensions which were used to generate the geometry. Where values were not specified appropriate approximates were used.

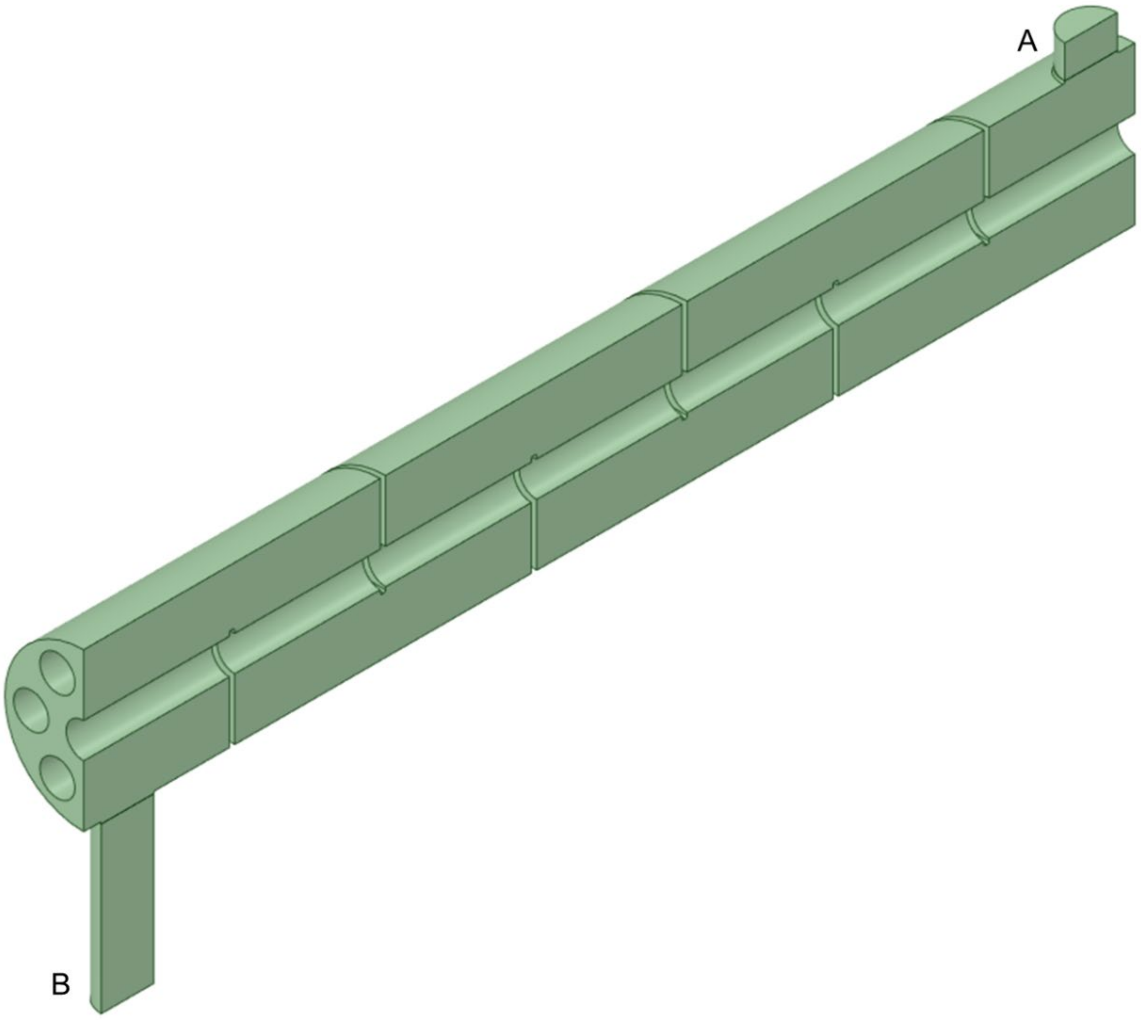

Figure 3: Half model of the validation case geometry with the shell inlet (A) and extended outlet (B) annotated

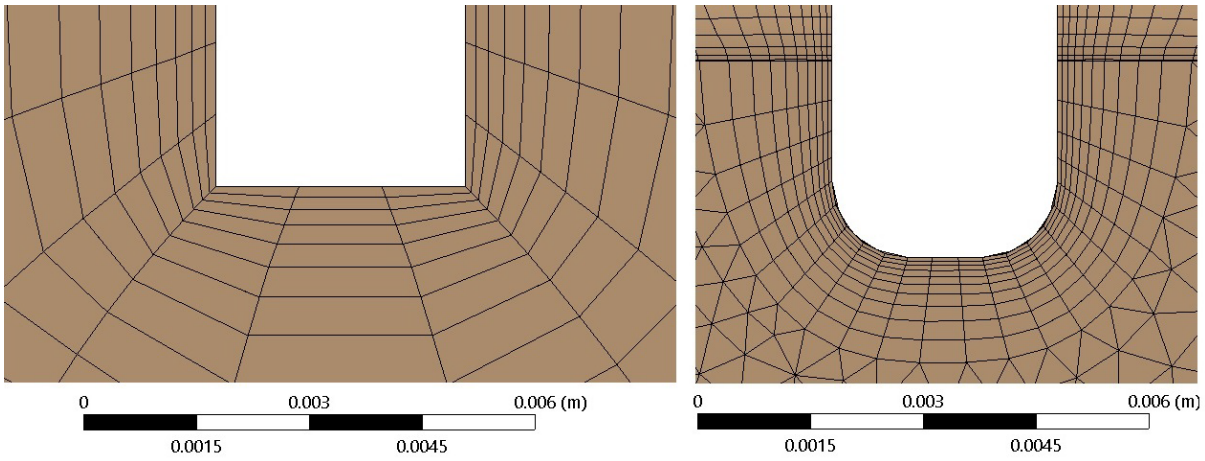

Figure 4: Mesh improvement from using fillet at baffle ends

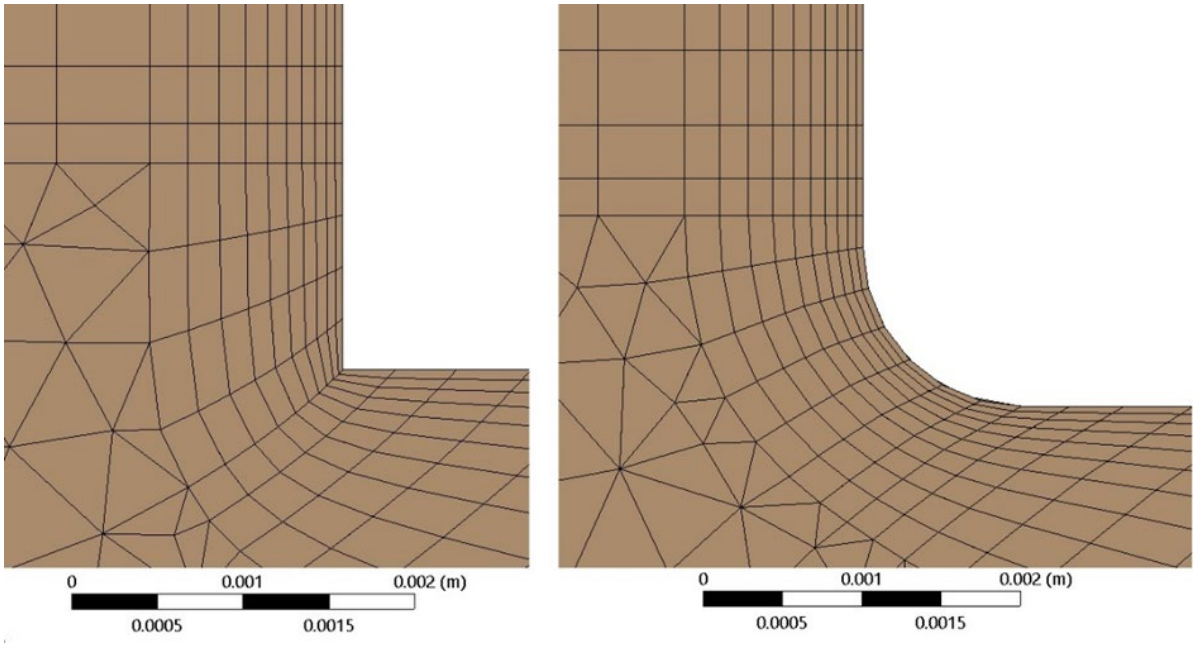

Figure 5: Mesh improvement from using fillet at shell inlet

Mesh generation

As no meshing method is stated within the article best practice CFD techniques were used. When a fluid passes over the tubes and encounters the shell walls a boundary layer will form. For the tubes, a thermal boundary layer is also present. Hence, it is necessary to have appropriate mesh elements in these areas to represent the fluid behaviour. Having sufficiently accurate mesh resolution in the boundary layer effects the accuracy of the solution (Tu, Yeoh and Liu, 2007).

Within ANSYS CFX the inflation layer option is used for boundary layer meshing. The smooth transition option uses the local element size to calculate the first layer thickness so that the rate of change is smooth (ANSYS, 2010). Combined with face sizing's on the shell and tube walls the first layer thickness can be controlled. When smaller face sizing's were introduced, smaller elements were generated to blend the final inflation layer into the global element size (Figure 6). This helped increase the mesh density in areas where the inflation layers were restricting the free stream elements. Figure 7 shows the increase in elements in the free stream flow by reducing the face sizing's.

The element size specified for the face sizing's were not uniform across all the surfaces. In areas with large amounts of change, such as the baffle ends, smaller face sizing's were used to better capture the flow. The inlet and outlet were meshed with sweep methods as there is unlikely to be any changes to the flow in the horizontal direction. Mesh settings are specified in Appendix C.

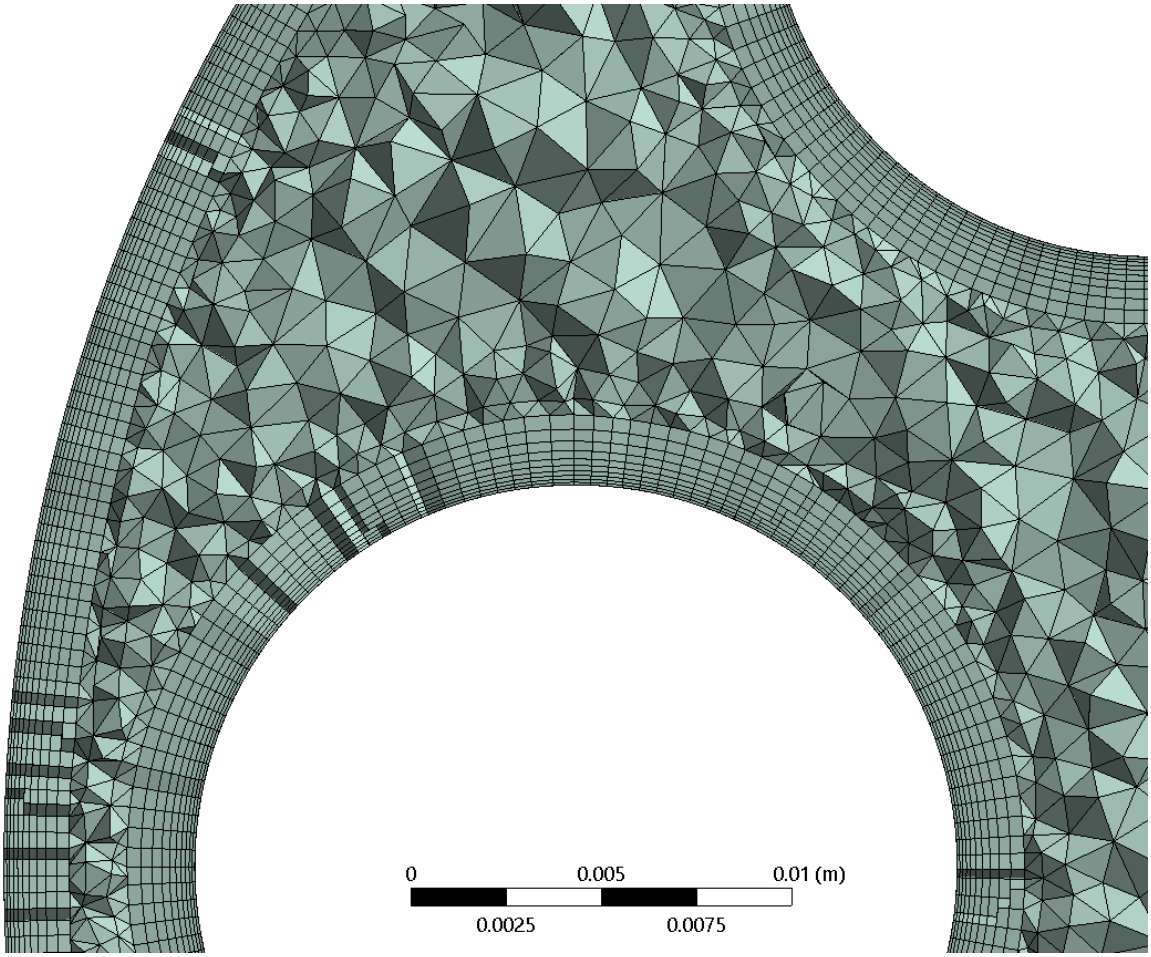

Figure 6: Mesh generated with 0.45mm face sizing showing the smooth blend of elements from the boundary layer to the free stream flow

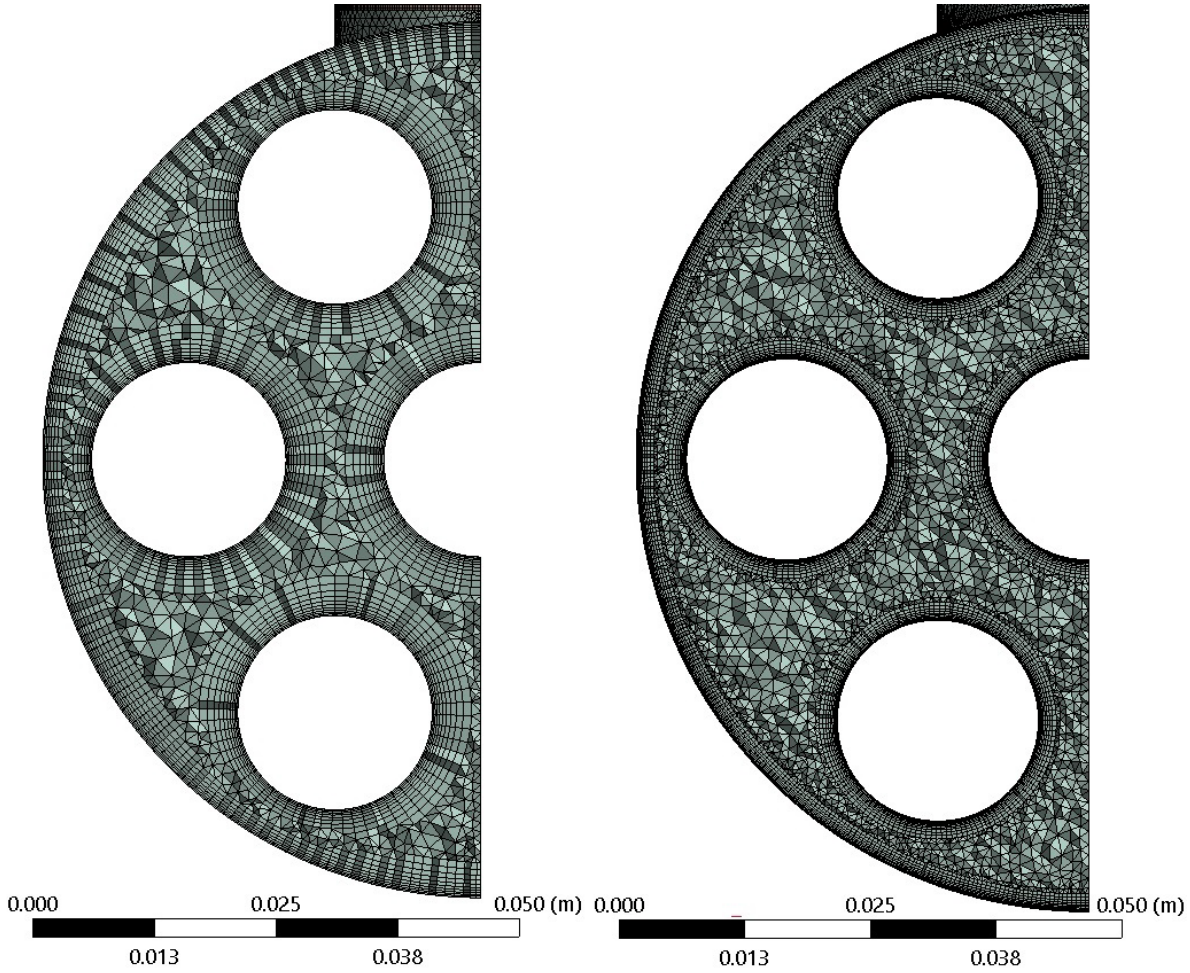

Figure 7: Improvement of elements in the free stream flow with smaller face sizing's

Pre-processor setup

Turbulence model

Throughout the literature the most common turbulence model is the k-ϵ model with the validation article suggesting the realizable k-ϵ model. The stability, robustness and simplicity of the model makes it a good workhorse and general default model for predicting turbulent flow (Tu, Yeoh and Liu, 2007). However, it is unable to accurately predict flow separation and stall characteristics (Menter, 2009). Within a heat exchanger the flow pattern causes cross flow across the tube bundle where separation occurs suggesting that the k-ϵ model is not appropriate.

Another turbulence model, the k-ω, is more accurate in the viscous sublayer and in flows with adverse pressure gradients but is very sensitive to the specified free stream values (Menter, 2009). The realizable k-ϵ model used in the validation case is a more developed version of the standard k-ϵ and provides more accurate results (Tu, Yeoh and Liu, 2007).

The shear-stress transport (SST) model combines the best elements of the k-ϵ and k-ω models. This model uses functions which gradually blend the different elements

together (Menter, 2009). Eggenspieler (2012), suggest that the SST model is an accurate two-equation model for separation prediction. (Batalha Leoni, Suaiden Klein & de Andrade Medronho, 2017) compare the k-ϵ and SST turbulence model on a shell and tube heat exchanger. They conclude that the SST model provides a greater accuracy when predicting the flow characteristics and heat transfer effects.

Compared to k-ϵ the SST model will require more computational power and greater mesh resolution in the boundary layer. Tu, Yeoh and Liu (2007) suggest that there should be 8-10 nodal points in the boundary layer and a Y+ of approximately 1 for low Reynolds flows. Y+ is a dimensionless distance of the first node distance from the wall and is used to measure the quality of the boundary layer mesh (ANSYS, 2009). Though more computationally expensive the SST model will perform better than the k-ϵ model and therefore will be used instead.

Other settings

Initially a steady state simulation was conducted with Figure 8 illustrating the applied boundary conditions.

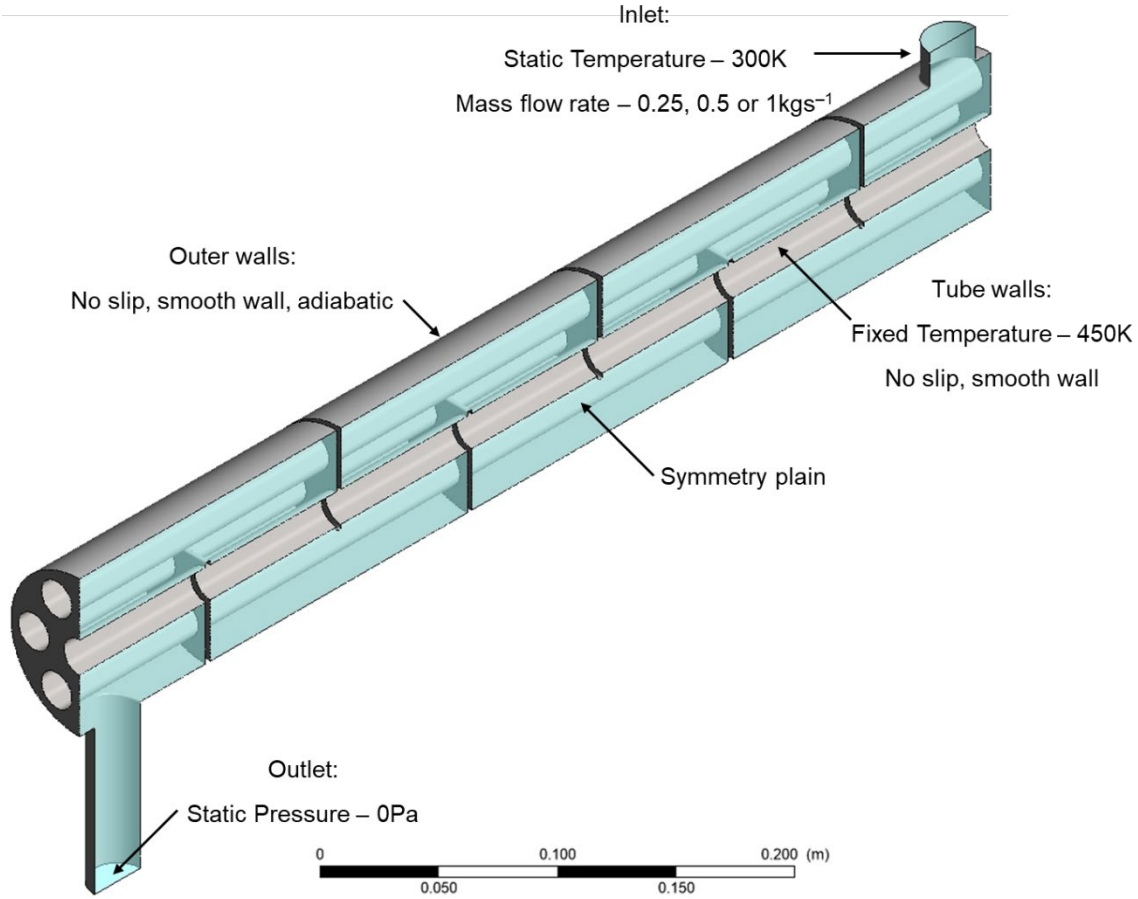

Figure 8: Validation case applied boundary conditions

The thermal energy heat transfer option was selected as the flow is incompressible (ANSYS, 2011). The SST turbulence model was used with all relating settings set to default. The root mean squared, RMS, residual target is set at $1x10^{-4}$. This value is

relatively loose but is sufficient for many engineering applications (ANSYS, 2011). The maximum iteration limit of 500 was applied with the timescale control set to automatic. Monitors were used to assess the shell outlet bulk temperature and pressure drop. As only half of the geometry is being modelled the inlet mass flow rate is halved. Therefore, the input values are now 0.25, 0.5 and 1kgs^{-1} compared to Table 1. The inlet turbulence intensity is not specified hence will be set at medium as recommended by (ANSYS, 2011).

Mesh sensitivity study

To assess the quality of the mesh a mesh sensitivity study was carried out. The 0.25kgs^{-1} shell input was selected, and the number of nodes generated ranged from 3.32 to 26.06 million. At 26.06 million nodes the memory limit was reached for the computers being used. Refinements of the mesh were carried out by decreasing the face sizing applied to the shell and tube walls. Appendix C sets out the mesh parameters for each case. All the simulations were run to 500 iterations with the shell outlet bulk temperature being calculated using the arithmetic mean of the last 300 iterations. Y+ was also assessed with data being gathered for the tube and shell walls.

Shell bulk outlet temperature

Figure 15 shows the outlet bulk temperature for each of the meshes where the values are converging with an increasing number of nodes. This gives an initial confidence in the quality of the mesh. Table 2 presents the output data.

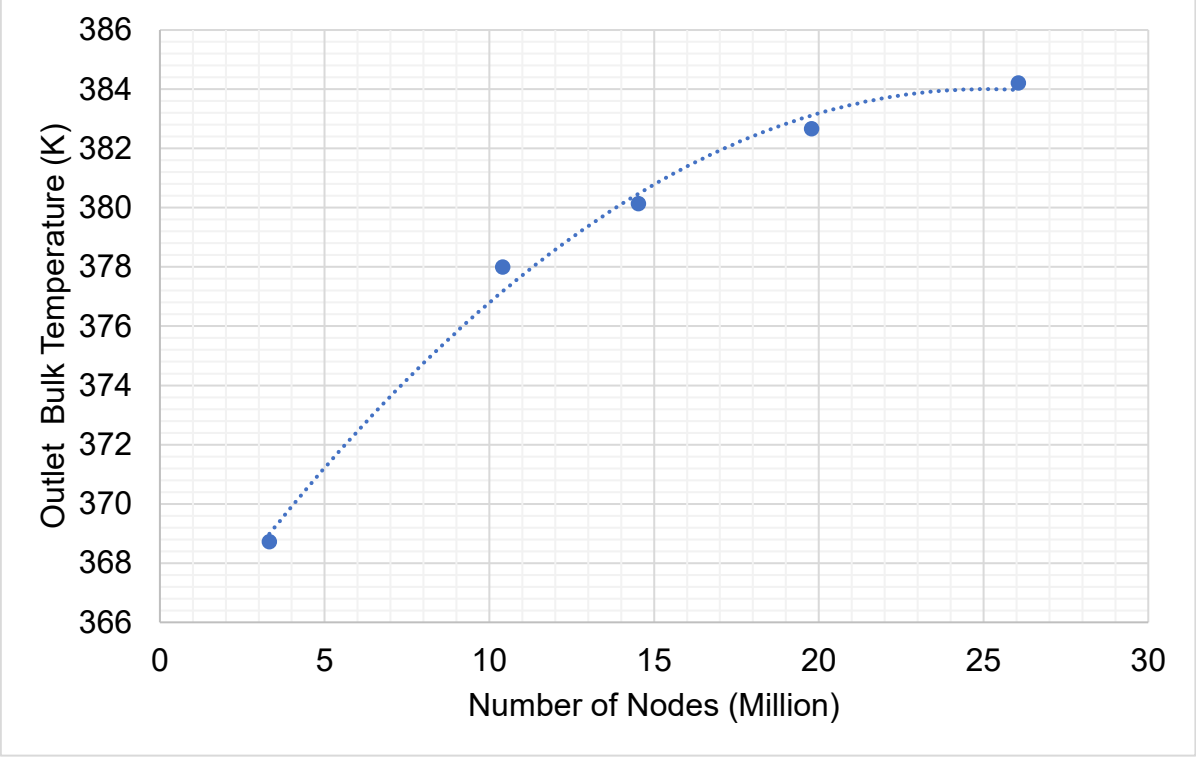

Figure 9: Validation case mesh sensitivity outlet bulk temperature results

Table 2: Bulk shell outlet temperature: Mesh sensitivity study

Nodes (Million)	Outlet temperature (K)
3.32	368.72
10.41	378.00
14.53	380.13
19.78	382.67
26.06	384.21

Y+ results

When assessing the Y+ values the maximum value, average and the percentage of nodes where Y+ > 5 were looked at. Though one is the ideal value for Y+ five was selected to illustrate the improvement of the mesh. Figure 10 and Figure 11 show the results for the shell and tube walls where with increasing number of nodes all the parameters reduce. Compared to the shell walls the number of nodes with a Y+ > 5 is on average 23% greater for the tube walls. This suggests that the boundary layer is being resolved better at the shell walls.

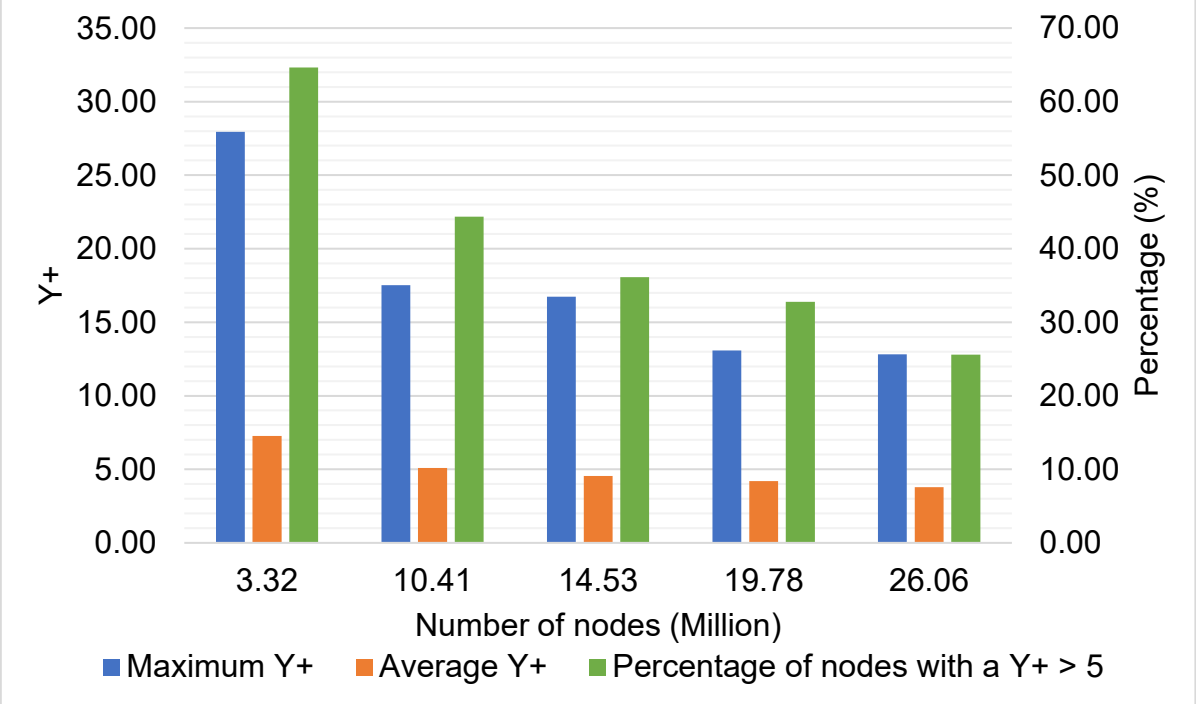

Figure 10: Y+ data vs. number of nodes (Million) for shell walls

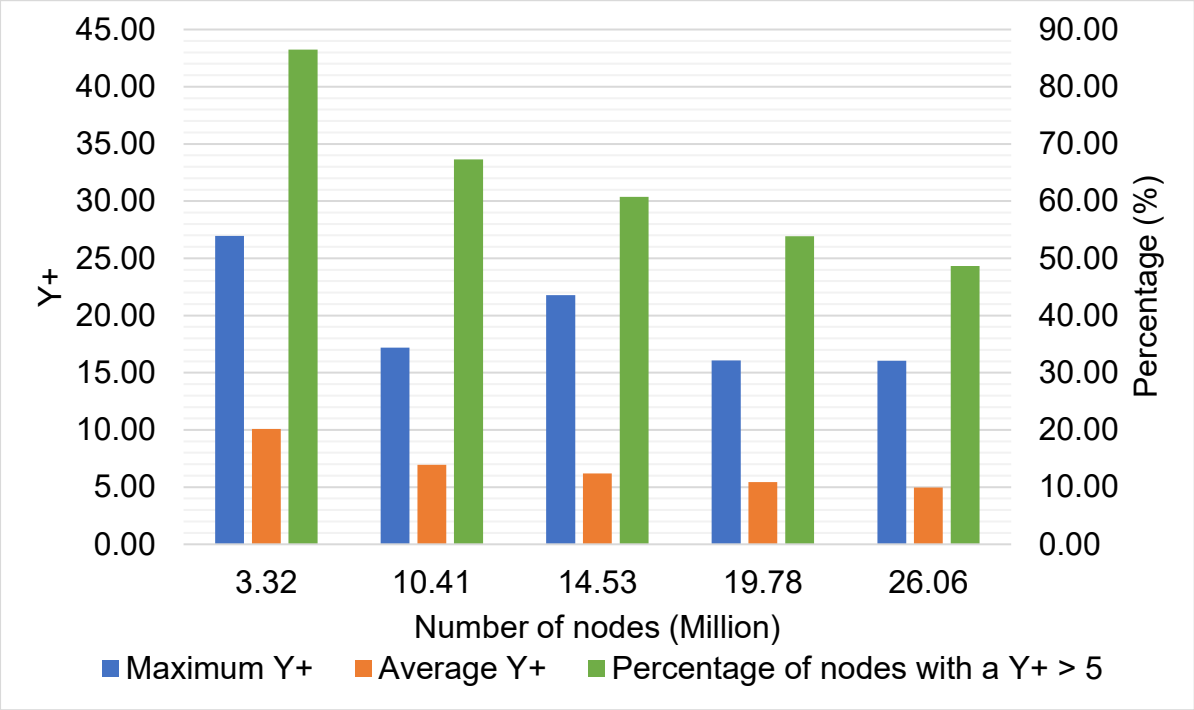

Figure 11: Y+ data vs. number of nodes (Million) for tube walls

For the shell and tube walls at the 19.78 and 26.06 million node case the maximum Y+ values stabilised. This is explained by the presence of localised pockets producing higher Y+ values (Figure 12).

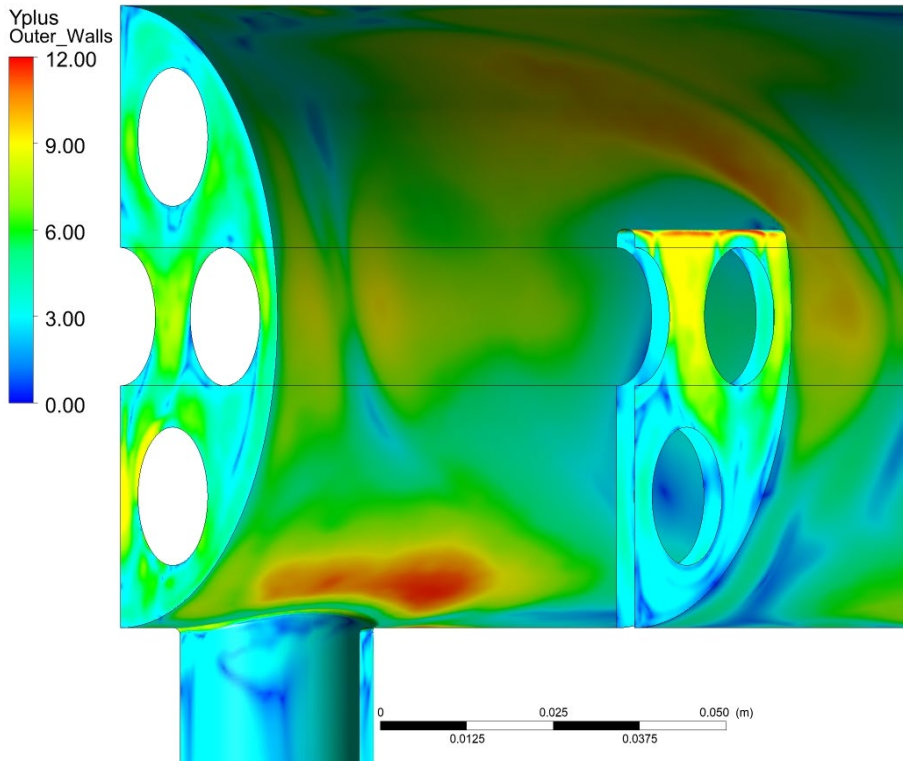

Figure 12: Y+ plotted results on shell walls for the 26.06 million node case where localised pockets of higher Y+ values are present

It can also be noted that the average also stabilises at the larger node cases. This would suggest that face sizing's are no longer reducing the Y+ values. To solve this a different mesh method could be used. For example, specifying a first layer thickness and calculating the number of inflation layers would reduce the first layer thickness and thus the Y+ values. Further, a more efficient use of localised improvements will reduce the maximum Y+ values.

Transient analysis

When analysing the results from the mesh sensitivity study, it was noted that poor convergence was being achieved. The turbulence, momentum and mass residuals were all between $1x10^{-3}$ and $1x10^{-4}$ and the heat transfer residual oscillated around $1x10^{-4}$. This convergence did not meet the criterium specified by the pre-processer, so all simulations ran to the 500-iteration limit. Figure 13 shows the oscillatory nature of the last 300 iterations of bulk outlet temperature from the mesh sensitivity study. The oscillatory nature and poor convergence suggest that the flow contains periodic oscillations and is thus a transient problem. This behaviour is not unexpected due to flow separation over the tube bundle caused by crossflow.

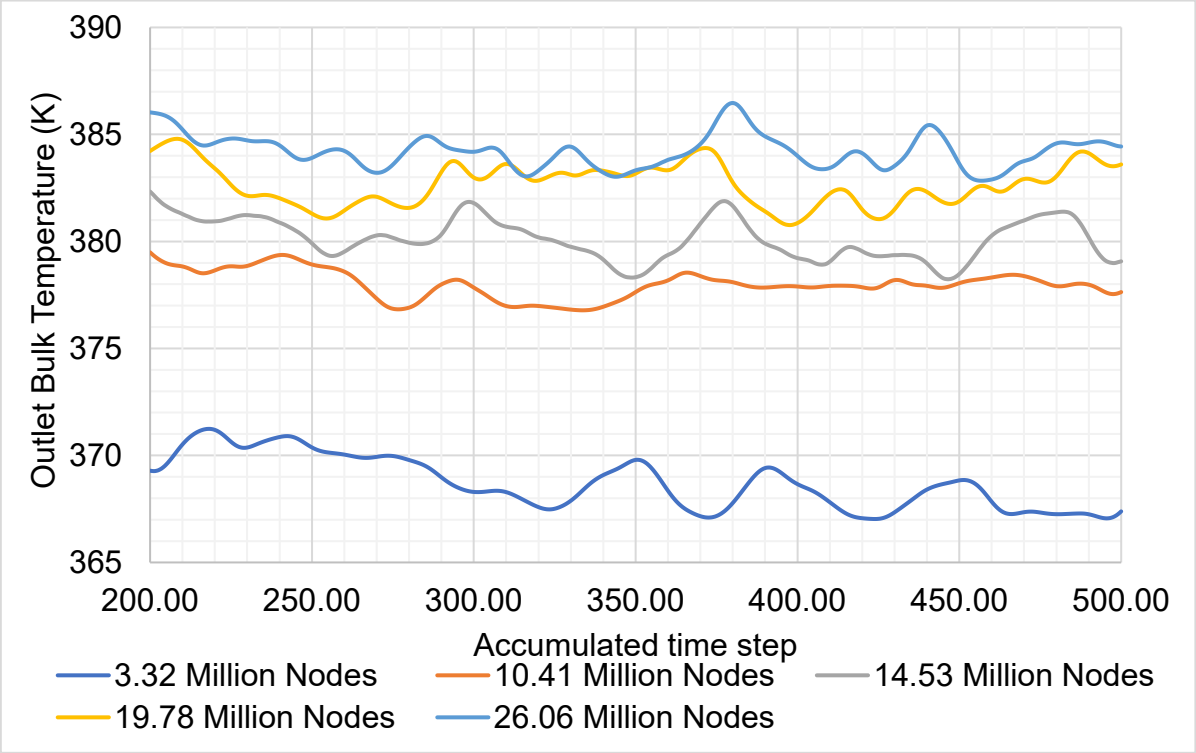

Figure 13: Outlet temperature from the last 300 iterations of the mesh sensitivity study

Timestep selection

A 1 baffle version of the heat exchanger was modelled to assess a suitable timestep for the model. The initial timestep was selected using the Strouhal number which is a non-dimensional number used to characterise period flow. Equation 6 defines Strouhal number with the shell average velocity being calculated from the steady state results. Katopodes, 2019 presented the relationship between Reynolds number

and Strouhal number. This allowed values for Reynolds number from the Bell-Delaware method to be used to approximate a Strouhal number of 0.2. Solving the equation allowed the oscillation frequency and thus oscillation period to be determined. Using the oscillation period as an initial timestep an adaptive timestep was used with the aim of achieving between 2 and 5 coefficient loops per timestep. The adaptive timestep converged to a value of 0.03s. This timestep was used in all simulations with a simulation time of 10s. Ideally a longer time would be simulated allowing a steady state solution to be obtained. Due to larger computational demand and quantity of iterations simulations were run on a more powerful CPU intensive virtual computer. However, this had a lower memory limit so could only run a 14.53 million node case. As shown by Figure 9 this will result in an underprediction of the results as this mesh is not fully independent.

Equation 6
(Douglas, 2011)

$$S_{tr} = \frac{f_o d_{to}}{u_a}$$

Where:

S_{tr} – Strouhal number (n/a)
f_o – Oscillation frequency (s^{-1})
d_{to} – Tube outside diameter (m)
u_a – Average shell velocity (ms^{-1})

Results

Figure 14 presents the bulk outlet temperature monitor plots for the 0.5, 1 and 2kgs^{-1} simulation up to a time of 10s.

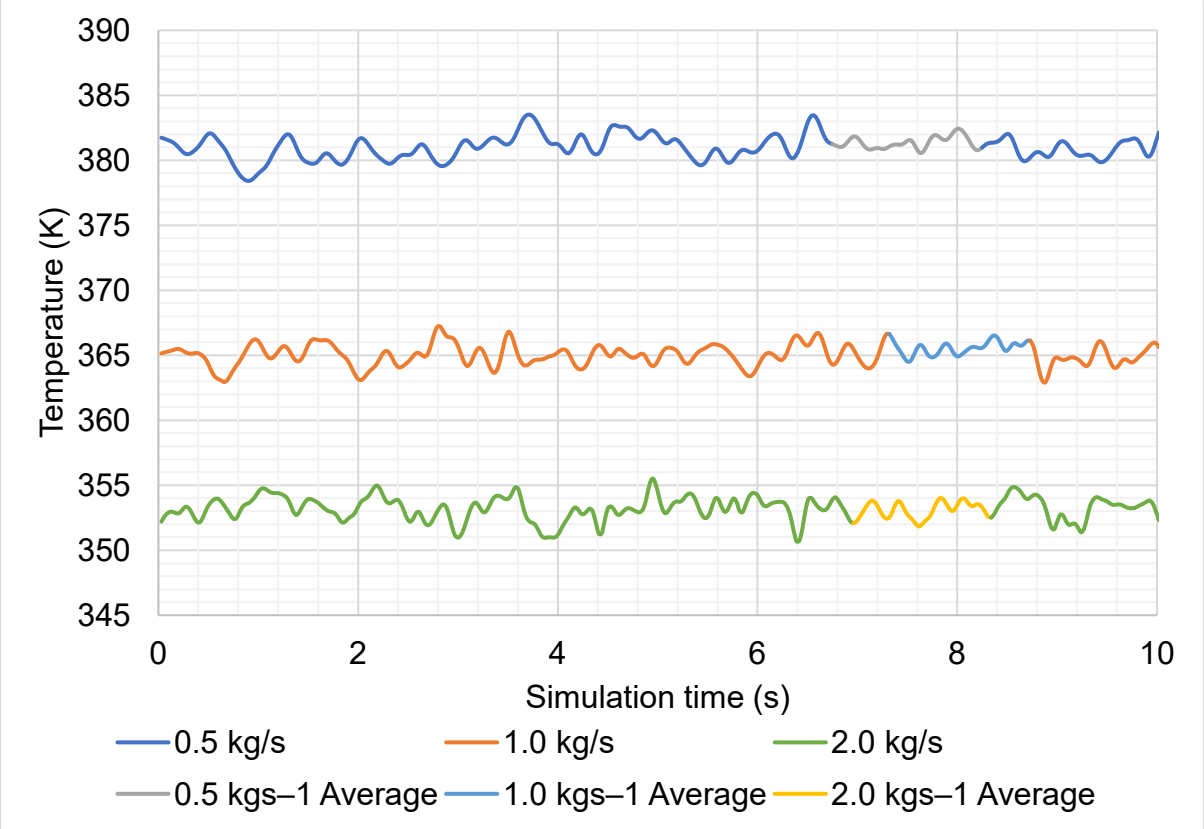

Figure 14: Bulk outlet temperature vs. simulation time for validation case simulations

Due to the oscillatory nature average outlet temperatures were determined (Table 3). Averages were selected by looking at the most settled areas of fluctuations. Using the determined average, the value for U was calculated (Table 4). For the LMTD Equation 3 was applied with the tube temperature terms set to zero resulting in Equation 7. The full calculation method is set out in appendix C.

Table 3: Bulk shell outlet temperatures: Validation case

Mass flow rate (kgs^{-1})	Outlet temperature (K)		Percentage difference (%)
	Current paper	Ozden and Tari	
0.5	381.34	340.40	12.03
1.0	365.56	330.18	10.72
2.0	353.09	326.64	8.10

Table 4: U results: Validation case

Mass flow rate (kgs^{-1})	U ($Wm^{-2}K^{-1}$)		Percentage difference (%)
	Current paper	Ozden and Tari	
0.5	6294.92	2514	150.39
1.0	9248.58	3757	146.17
2.0	14056.16	6768	107.69

Equation 7

$$\Delta T_{\ln\_val} = \frac{(T_w - T_{o)} - (T_w - T_i)}{\ln\left(\frac{T_w - T_o}{T_w - T_i}\right)}$$

Where:

$\Delta T_{\ln}$ – Log mean temperature difference (K)
T_w – Tube wall temperature (K)
T_o – Shell outlet temperature (K)
T_i – Shell inlet temperature (K)

Discussion

Figure 15 compares the calculated values of the overall heat transfer coefficient from the current study (Table 4) and from the article by Ozden and Tari (2010) (Table 1). The current simulations overpredict their results by 108–150%. There are various weaknesses in the CFD theory applied by Ozden and Tari (2010). The main flaws are the number of mesh elements used and the turbulence model selected.

Their mesh was generated using Gambit software, part of ANSYS FLUENT, and produced a 1.36 million element mesh. In this study, using different software, a 14.53 million node mesh was used correlating to 34.54 million elements. Though different software was used the large disparity in the number of elements suggests that their study did not have a sufficient mesh resolution. As shown by the mesh sensitivity study with increasing mesh nodes the bulk outlet temperature increased further from

the 340.40K outlet temperature obtained by Ozden and Tari (2010). Additionally, initial running using very coarse meshes produced the closest results to theirs.

The realizable k-ϵ model used in the validation article is not as suitable as the SST model when predicting the flow characteristics within a heat exchanger. However, in the current simulations the advantages of the SST model are not being fully utilised. The criterium of a Y+ ≈ 1 across all nodes was not met for the 14.53 million node mesh used or any of the meshes in the mesh sensitivity study. Therefore, further mesh improvements are needed to ensure the full utilization of the SST model. As Y+ is related to the flow velocity conducting the mesh sensitivity study at the maximum flow rate would also be suggested to ensure that the most optimal mesh is applied for all simulations.

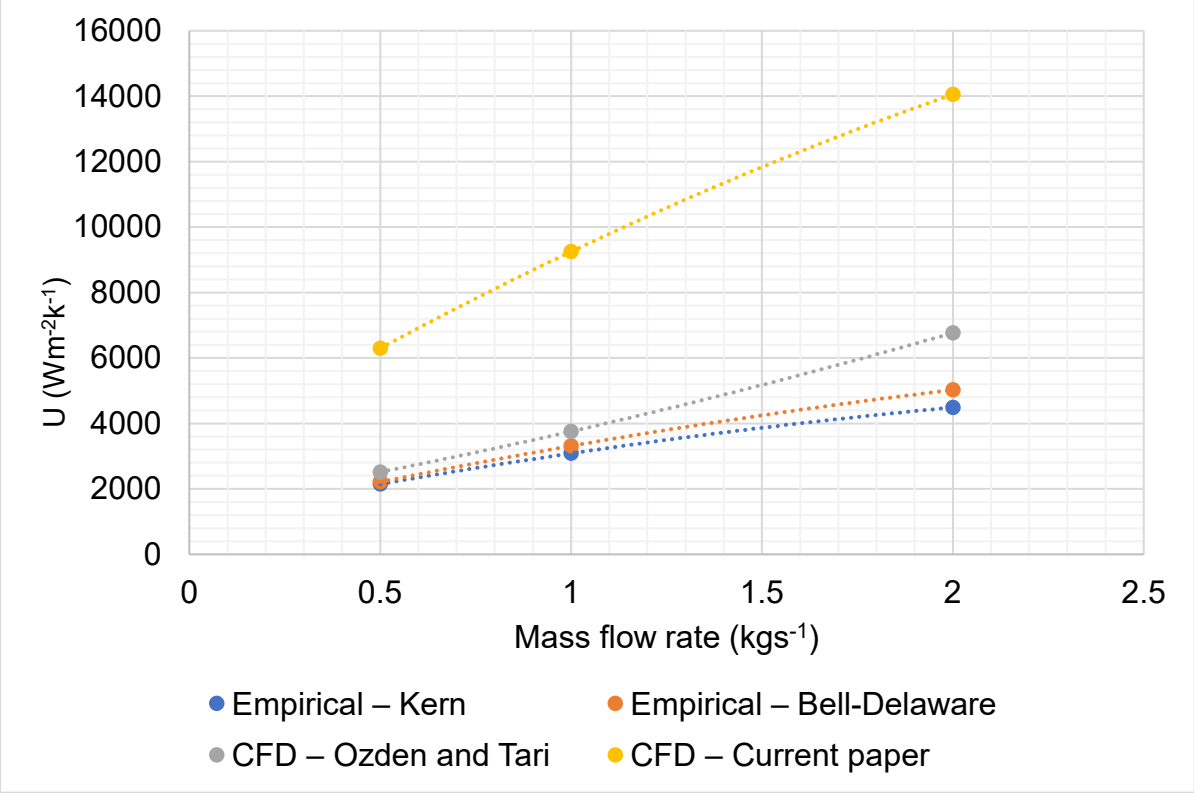

Figure 15: U vs. mass flow rate for the Kern, Bell-Delaware, article CFD and validation CFD

A default convergence criterium was met in the validation case article. Within this study the steady state analysis did not converge to an accurate solution. Thus, a transient analysis was used where the convergence residuals improved. As illustrated by Table 5 the average heat transfer residuals for the 0.5 and 1kgs^{-1} decreased below the 1x10^{-4} target with the 2kgs^{-1} case not meeting the criterium. Further, the momentum residuals for the 1 and 2kgs^{-1} case oscillated between 1x10^{-3} and 1x10^{-4} also not meeting the specified criterium. This suggests that while there was an improvement in the accuracy of the results further improvement is possible. The use of a fixed timestep for all simulations resulted in the poor convergence as it meant that at each timestep the maximum of 10 coefficient loops was reached. This

resulted in a cascading effect of poorly converged timesteps impacting the overall accuracy of the simulation. A smaller timestep or an adaptive timestep should have been used to improve the accuracy of the simulation.

Pressure drop was also monitored with the averaged results being shown by Table 6. The pressure drop obtained from the current simulations underpredicts theirs by 19-33% potentially explaining the additional heat transfer (Table 5). Changes in the dynamic pressure relate to changes in velocity. Hence, as their pressure difference was larger this suggest their outlet velocity was lower. Heat transfer, specifically convection, is related to velocity and thus reducing velocity will decrease heat transfer.

Table 5: Average heat transfer residuals

Mass flow rate (kgs^{-1})	Heat transfer residual average	
	Steady state[a]	Transient
0.5	$1.14x10^{-3}$	$7.97\ x10^{-5}$
1.0	$1.17\ x10^{-3}$	$9.57x10^{-5}$
2.0	$8.99\ x10^{-4}$	$1.68x10^{-4}$

[a] First 100 iterations excluded to allow residual to settle

Table 6: Δp results for the validation case and article data

Mass flow rate (kgs^{-1})	Δp (Pa)		Percentage difference (%)
	Validation case	Article	
0.5	1239.87	1522.00	-18.54
1.0	4628.89	6168.00	-24.95
2.0	16719.90	24963.00	-33.02

The magnitude of difference between the results suggests that there is a fundamental error in one of the simulations. For this study a courser mesh was used than ideal, but this would not bring the results within a suitable difference. However, the setup of the simulation for this study is an improvement on the validation article. Improvements for this study can also be implemented and overall, the simulation could be improved by modelling the tube-side flow to fully represent a heat exchanger.

Figure 16 shows a velocity vector plot presenting the flow pattern through the heat exchanger. Here the sinusoidal flow pattern can be seen alongside the ‘dead’ zones behind the baffles. This confirms that the flow regime is behaving as expected. The transient behaviour can be seen by Figure 17, Figure 18 and Figure 19 confirming that the flow field is changing with time. These images were generated on the symmetry plain between the baffles marked on Figure 16.

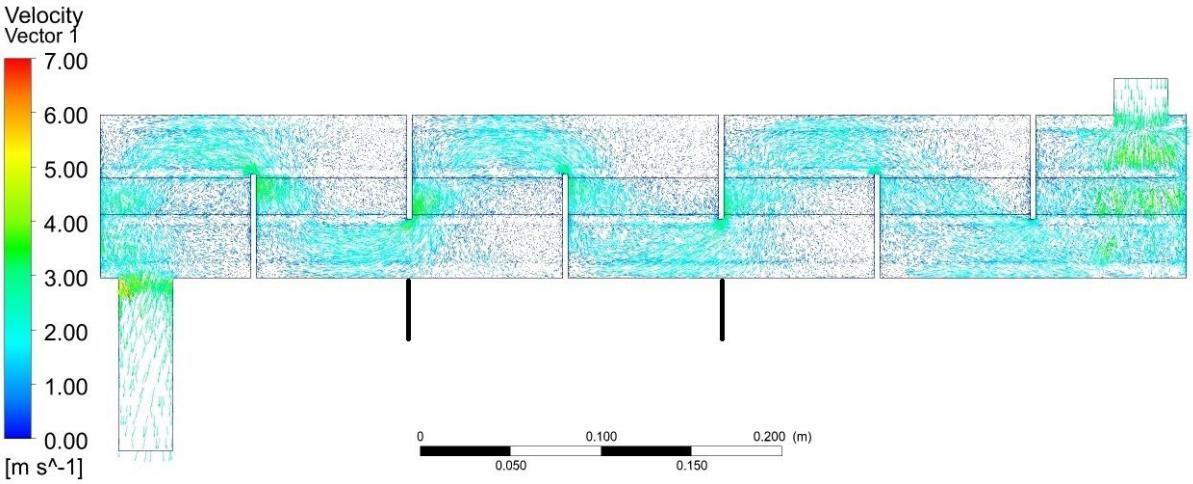

Figure 16: Vector plot demonstrating the sinusoidal flow pattern for the 2kgs^{-1} simulation

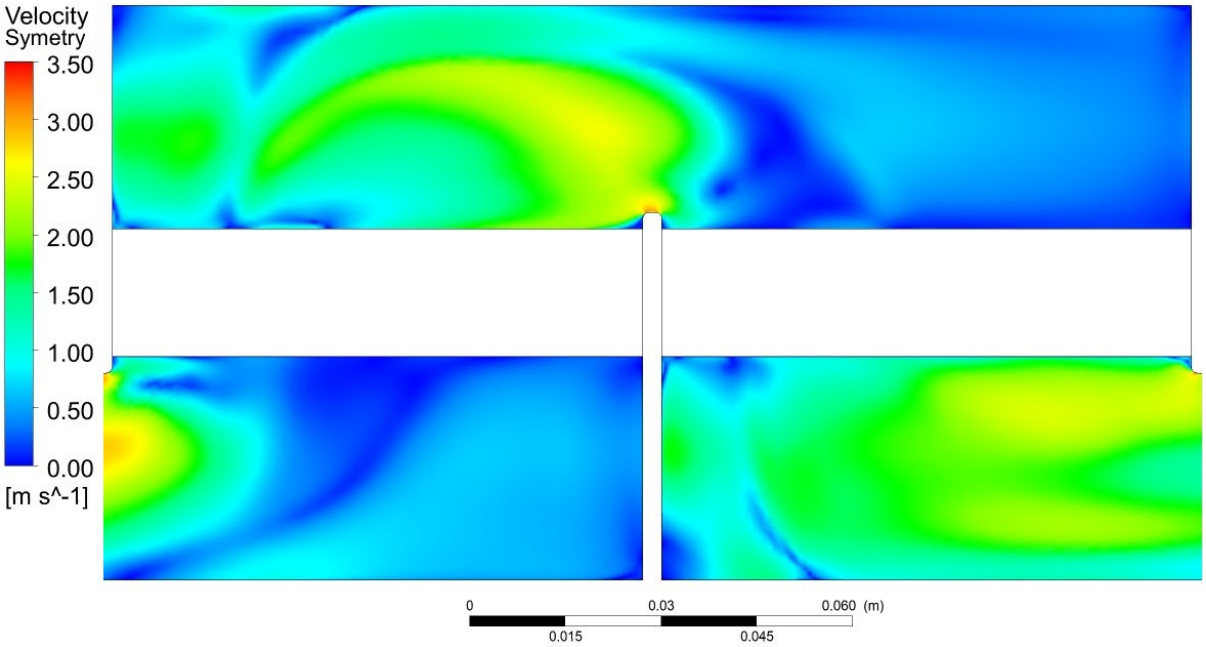

Figure 17: Velocity plot on symmetry plain for the 2kgs^{-1} simulation at t = 0s

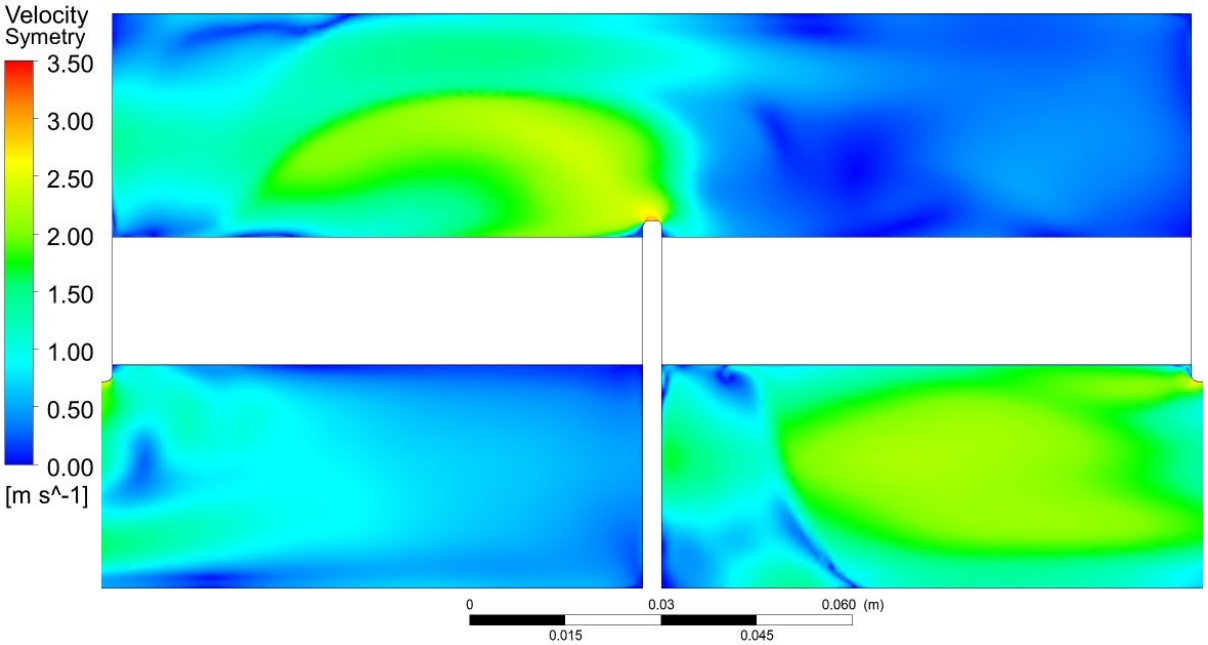

Figure 18: Velocity plot on symmetry plain for the 2kgs^{-1} simulation at t = 5s

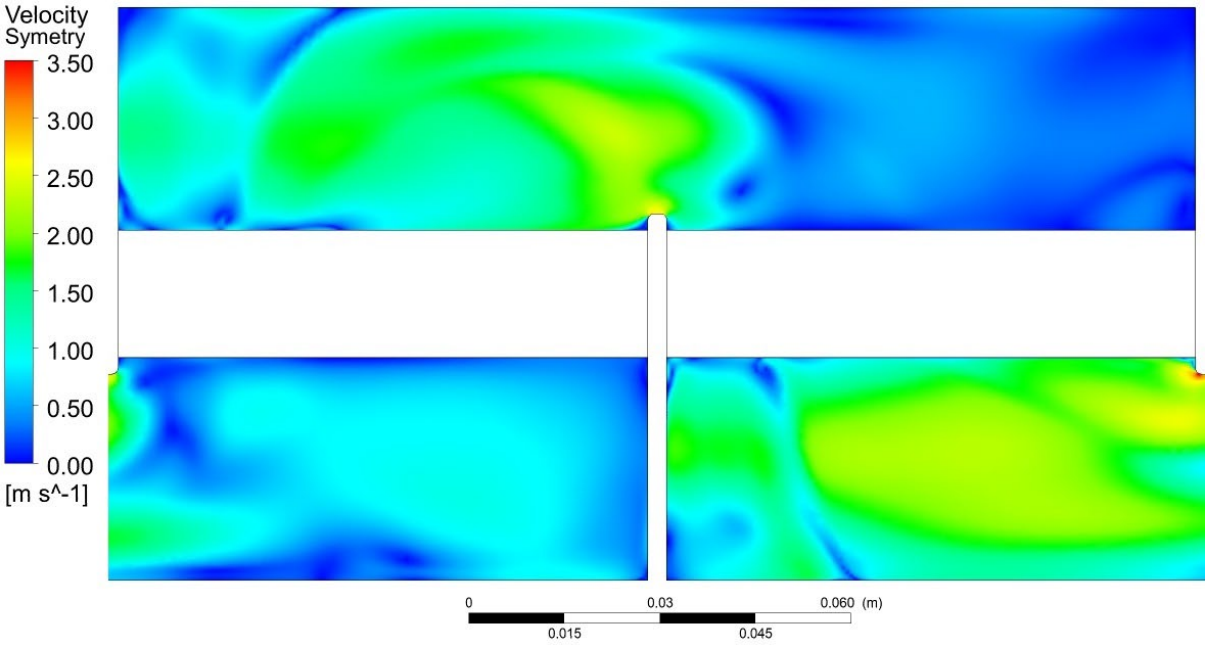

Figure 19: Velocity plot on symmetry plain for the 2kgs^{-1} simulation at t = 10s

University Heat Exchanger

In this section all three analytical methods will be conducted with the methods compared at the end. The university heat exchanger is a TECQUIPMENT TD360C shell and tube heat exchanger. Figure 20 shows the experimental apparatus where the heat exchanger is connected to the service module. Quick connectors connect the hot (Tube) and cold (Shell) fluid allowing the operation of both parallel-flow and counter-flow configurations. With closer inspection of the heat exchanger leakage paths around the baffles can be seen alongside corrosion and fouling on the heat transfer surfaces. Figure 20 demonstrates the leakage paths present where baffle-to-shell (Purple circle) and baffle-to-tube leakage (Orange circle) are shown.

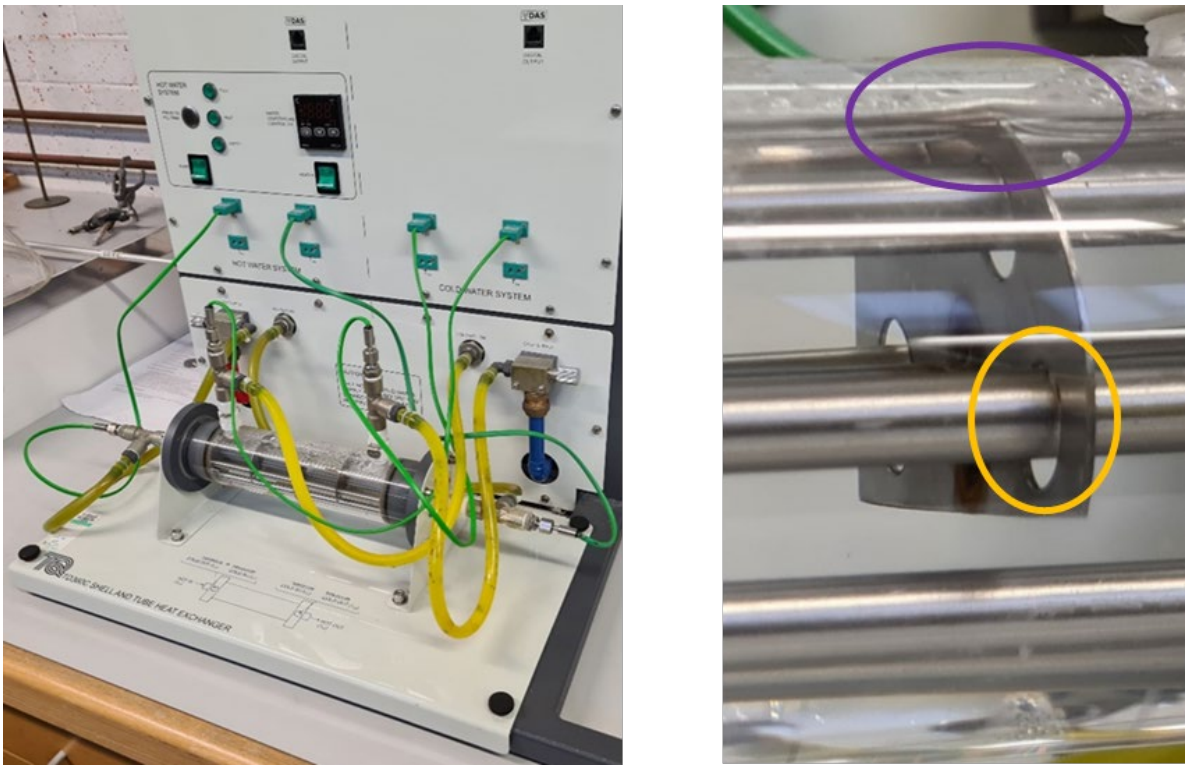

Figure 20: UHX connected to service module and baffle leakage paths present

Experimental process

A constant volumetric flow rate of 3Lmin^{-1} was set for the tube side flow with a temperature of approximately 60°C (333.15K). On the shell side mains water was used with volumetric flow rates of 0.5, 1, 2 and 3Lmin^{-1}. Using the experimental method both the parallel-flow and counter-flow configurations were run. Due to restrictions limiting access to the UHX experimental data was collated from the previous year's thermodynamics module when restrictions were not in place. Five sets of data were obtained with outliers identified and omitted. Appendix D contains more information on the experimental process including the geometric properties, experimental method, experimental temperature profiles and U calculation method.

Table 7: U results: Experiment, UHX

Shell volumetric flow rate ($Lmin^{-1}$)	U ($Wm^{-2}K^{-1}$)		Percentage difference (%)
	Parallel-flow	Counter-flow	
0.5	720.05	747.18	3.77
1.0	857.62	893.17	4.15
2.0	1147.45	1101.41	-4.01
3.0	1309.53	1249.33	-4.60

Empirical calculations

Before being applied to the UHX geometry the empirical calculations were validated against the values calculated by Ozden and Tari (2010). Their previous study, Ozden (2007), provides details on the correction factors they used when applying the Bell-Delaware method. Compared to their calculations the percentage difference was 0.32-1.82% for the Kern method and -0.21-0.09% for the Bell-Delaware method. The difference in the results is caused by different values for the temperature dependent variables.

As the methods had been validated, they were applied to the UHX geometry. Compared to the validation case setup the UHX models the tube side flow. This meant for the Kern method the tube-side and tube-wall heat transfer coefficient could be calculated and incorporated into the calculation of U. As the Bell-Delaware method only looks at the shell side flow the addition of tubes has no effect on the calculations. However, the correction factors were changed with the removal of the unequal baffle spacing correction factor and replacing it with the laminar flow correction factor. As shown by Figure 20 baffle leakage is present and there is a correction factor for it. However, it was not possible to quantify the exact dimensions of the leakage so this correction factor could not be included.

Results

Table 8 and Table 9 present the results from the Kern and Bell-Delaware methods. As the calculations are independent of the heat exchanger configuration the results are compared to the averaged values of the experimental results.

Table 8: Comparison of Kern and experimental U results: UHX

Shell volumetric flow rate ($Lmin^{-1}$)	U ($Wm^{-2}K^{-1}$)		Percentage difference (%)
	Experiment	Kern	
0.5	733.62	176.85	-75.89
1.0	875.40	234.01	-73.27
2.0	1124.43	303.18	-73.04
3.0	1279.43	349.70	-72.67

Table 9: Comparison of Bell-Delaware and experimental U results: UHX

Shell volumetric flow rate ($Lmin^{-1}$)	U ($Wm^{-2}K^{-1}$)		Percentage difference (%)
	Experiment	Bell-Delaware	
0.5	733.62	172.23	-76.52
1.0	875.40	302.69	-65.42
2.0	1124.43	537.86	-52.17
3.0	1279.43	691.26	-45.97

CFD analysis

While the CFD analysis did not confirm the accuracy of the CFD method it will be applied to the UHX to see how it performs against the experimental and empirical results. Once the model has been converted to the UHX geometry simulations will be run for both heat exchanger configurations at the four volumetric flow rates used in both the experimental and empirical methods.

Geometry

The geometry for the UHX was generated using the geometric properties presented in appendix D. Information on the geometric properties supplied by the manufacture were not complete resulting in some approximations when modelling the UHX. Geometric assumptions were made by only modelling the shell and tube fluid volume alongside the tubes. As with the validation case the shell outlet was extend by 40mm to prevent flow recirculation.

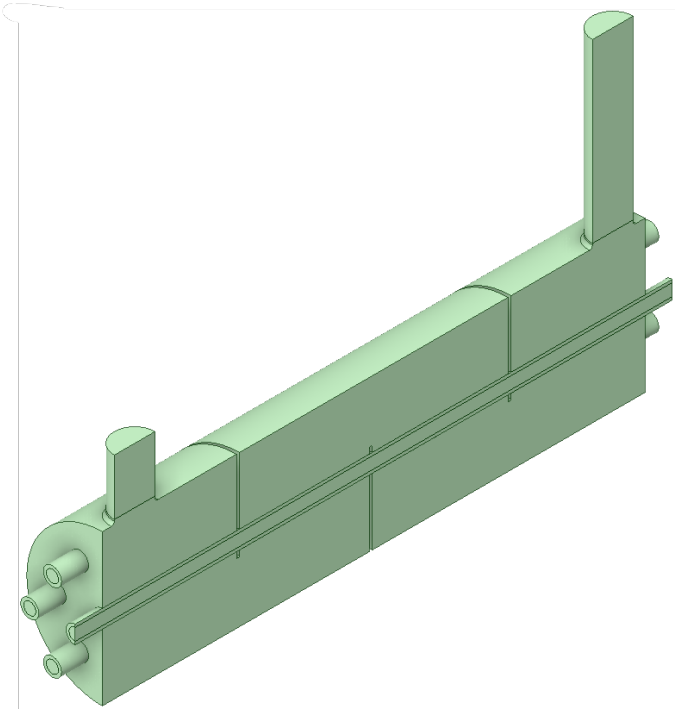

Figure 21: Half model of UHX geometry

Mesh

For the shell volume the mesh settings that generated the 14.53 million node mesh for the validation case were applied. These settings produced an 8.62 million node mesh. To represent the tubes and tube volume a sweep mesh was used. For the tube volume an inflation layer was used on the outer diameter to capture the boundary layer. For the tubes a face meshing method was used (Figure 22) to represent isothermal layers perpendicular to the direction of heat flow (Rogers, 1992). A summary of mesh settings applied are presented in Appendix D.

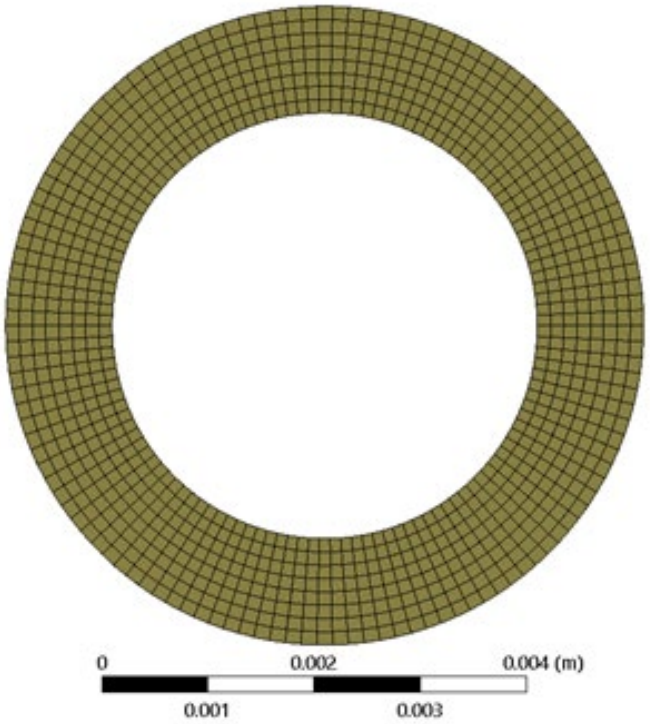

Figure 22: Tube meshing showing isothermal layers perpendicular to heat flow

Pre-processor

An improvement from the validation study was the implementation of an adaptive timestep. Using the Reynolds number values from the Bell-Delaware method 0.125s was approximated as the initial timestep using the Strouhal number equation. A lower limit of 1.25×10^{-2}s was initially set for the timestep. However, for the higher volumetric flow rate simulations this value was lower to 1×10^{-3}s allowing a suitable convergence. The convergence residual target was reduced to 1×10^{-5} which is sufficient for most engineering applications (ANSYS, 2011). Table 8 presents the final timesteps used for each simulation. As the timestep has been reduced significantly the total simulation time was decreased to five seconds.

Interfaces are used between all three domains with the conservative interface option applied. This allows the heat to flow between the boundaries (ANSYS, 2011). The average inlet temperature values were used for the shell and tube temperatures. Polynomial expressions were used the work out density based on the average tube and shell temperatures allowing the inlet mass flow rates to be determined. Figure 23 shows the boundary conditions for the parallel-flow configuration. For counter-flow the tube inlets and outlets were swapped. As the grade of stainless steel was

unknown ANSI304 stainless steel was used. Appendix D specifies the inlet conditions, and properties of the stainless steel used.

Table 10: Timesteps for UHX simulations

Shell volumetric flow rate ($Lmin^{-1}$)	Δt (s)	
	Parallel-flow	Counter-flow
0.5	$5.00x10^{-2}$	$5.12x10^{-2}$
1.0	$1.05x10^{-2}$	$1.50x10^{-2}$
2.0	$5.00x10^{-3}$	$1.00x10^{-3}$
3.0	$4.00x10^{-3}$	$1.00x10^{-3}$

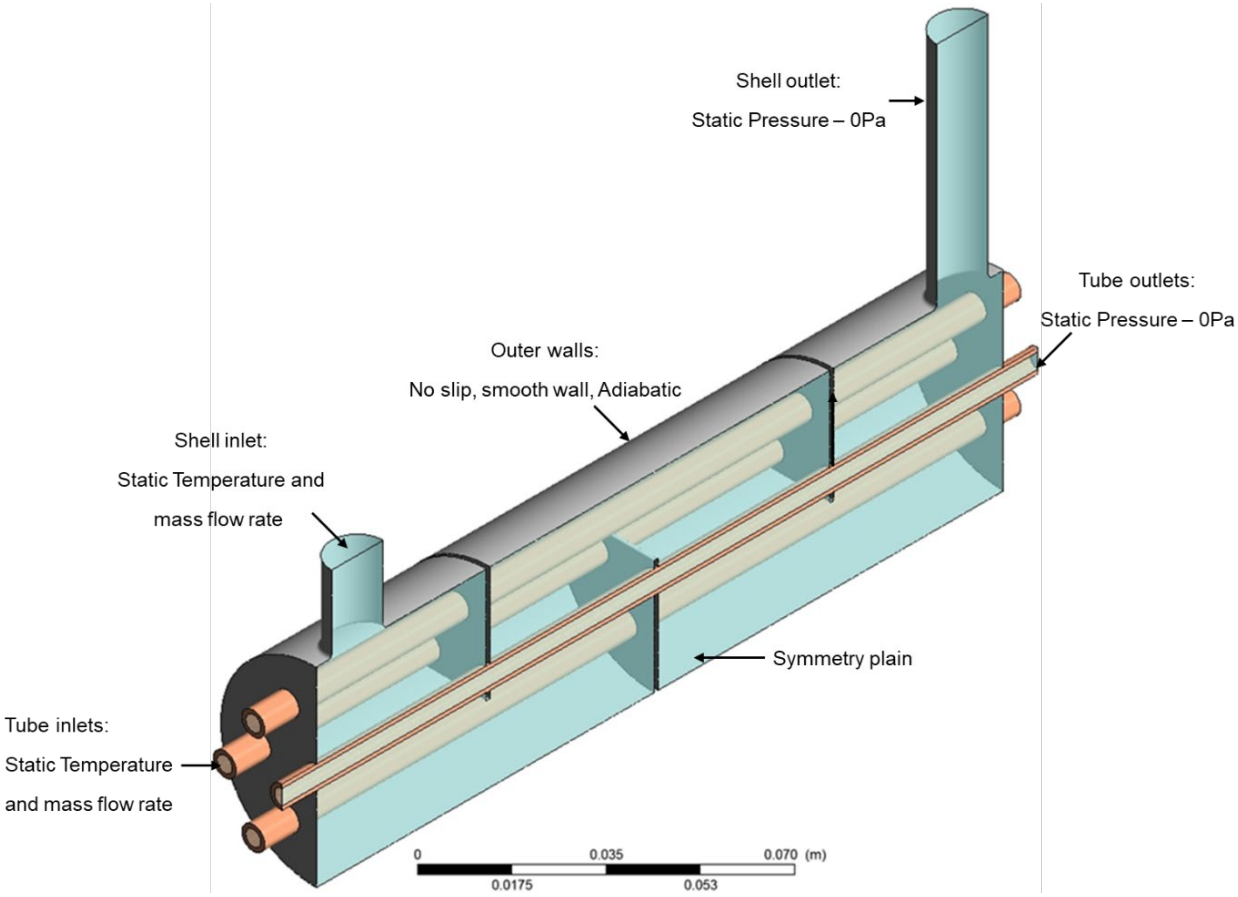

Figure 23: UHX boundary conditions

Results

Monitors were used to measure the changes in the shell and tube bulk outlet temperature. As with the validation case a suitable range of fluctuations were averaged to determine the outlet temperatures. Due to the variations in the timestep it meant that for the lower volumetric flow rate simulations less iterations were completed. Therefore, the potential oscillatory nature of the transient analysis was not present. For these cases, the averages were determined over the entire curve. The calculated values for U are presented by Table 11 and Table 12. The averaged outlet temperatures and U calculation method are presented in appendix D.

Table 11: Parallel-flow U results: CFD, UHX

Shell volumetric flow rate ($Lmin^{-1}$)	U ($Wm^{-2}K^{-1}$)		Percentage difference (%)
	Experiment	CFD	
0.5	720.05	838.80	16.49
1.0	857.62	1117.98	30.36
2.0	1147.45	1457.13	26.99
3.0	1309.53	1641.34	25.34

Table 12: Counter-flow U results: CFD, UHX

Shell volumetric flow rate ($Lmin^{-1}$)	U ($Wm^{-2}K^{-1}$)		Percentage difference (%)
	Experiment	CFD	
0.5	747.18	880.83	17.89
1.0	893.17	1172.75	31.30
2.0	1101.41	1493.10	35.56
3.0	1249.33	1694.80	35.66

Discussion

The results from the parallel-flow analysis are presented by Figure 24 with the counter-flow results shown by Figure 25. The parallel-flow and counter-flow results overpredict the experimental results by 16-30% and 18-36%. An overprediction of the results is not unexpected as the CFD geometry represents a perfect model when compared to the experimental results. Primarily, this is because the CFD model does not include leakage or fouling which is present in the experimental analysis.

In comparison the Kern and Bell-Delaware methods underpredict the experimental values by 73-76% and 46-77%. These methods both use empirical data which was collected for industrial sized heat exchangers. The UHX has been designed as an educational aid when teaching about heat exchangers. Therefore, in comparison to an industrial heat exchanger it is relatively small and has a simplified geometry. This means that the empirical methods are not designed to be used with this application. Looking at the requirements to apply the Kern method the correlation that was used to determine the Nusselt number specifies a Reynolds number greater than 2000.

For the UHX the values calculated for the Reynolds number were between 221 and 1143, showing how the UHX is outside the range that the empirical methods were designed for.

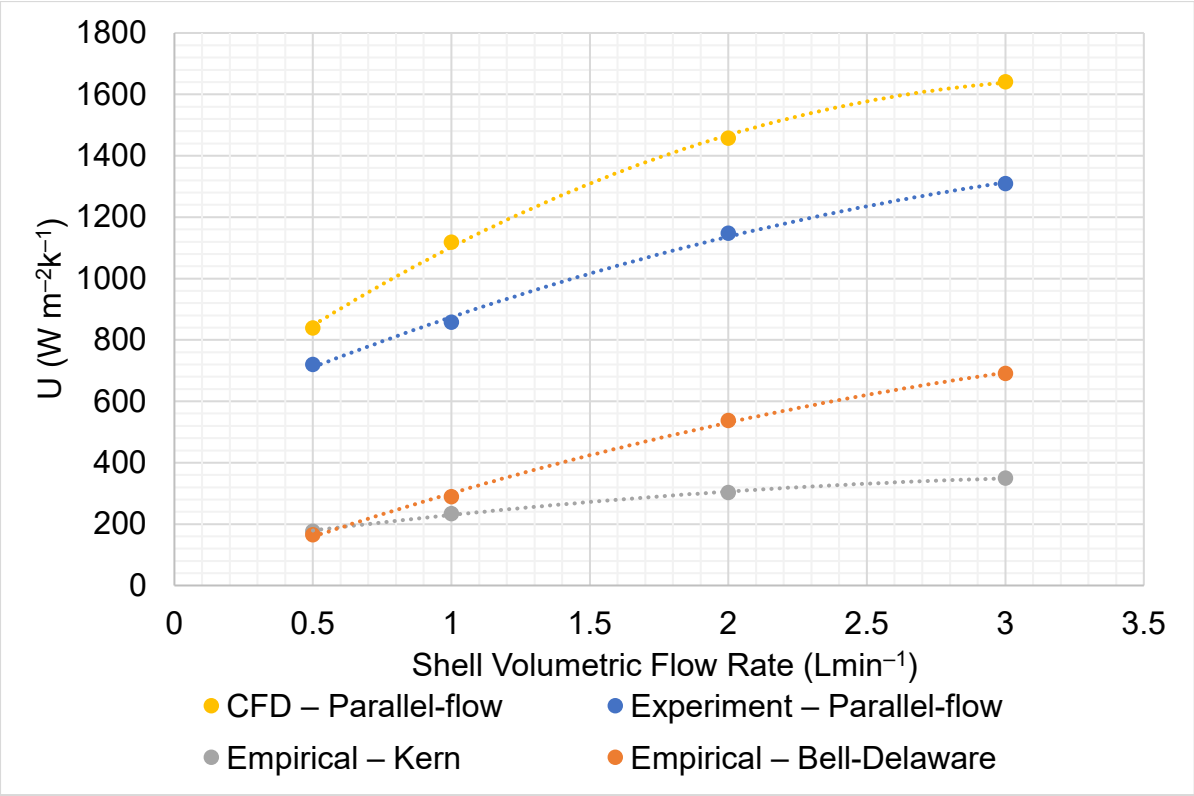

Figure 24: U vs. volumetric flow rate for the CFD, experimental, Bell-Delaware and Kern analyses – Parallel-flow

Data from previous years was collated to determine the experimental results under non-ideal experimental conditions. Therefore, a more rigorous experimental procedure is needed to determine accurate results. Further, other factors such as varying inlet temperatures, heat loss to the environment and inaccuracies in the thermocouple measurements will impact the accuracy of the results.

The difference between the two flow configurations in experimental results is -5-4% (Table 7) and 2-3% for the CFD analysis (Table 13). These small differences suggest that for this heat exchanger there is no advantage for either configuration. The proximity of the results can be seen by Figure 26.

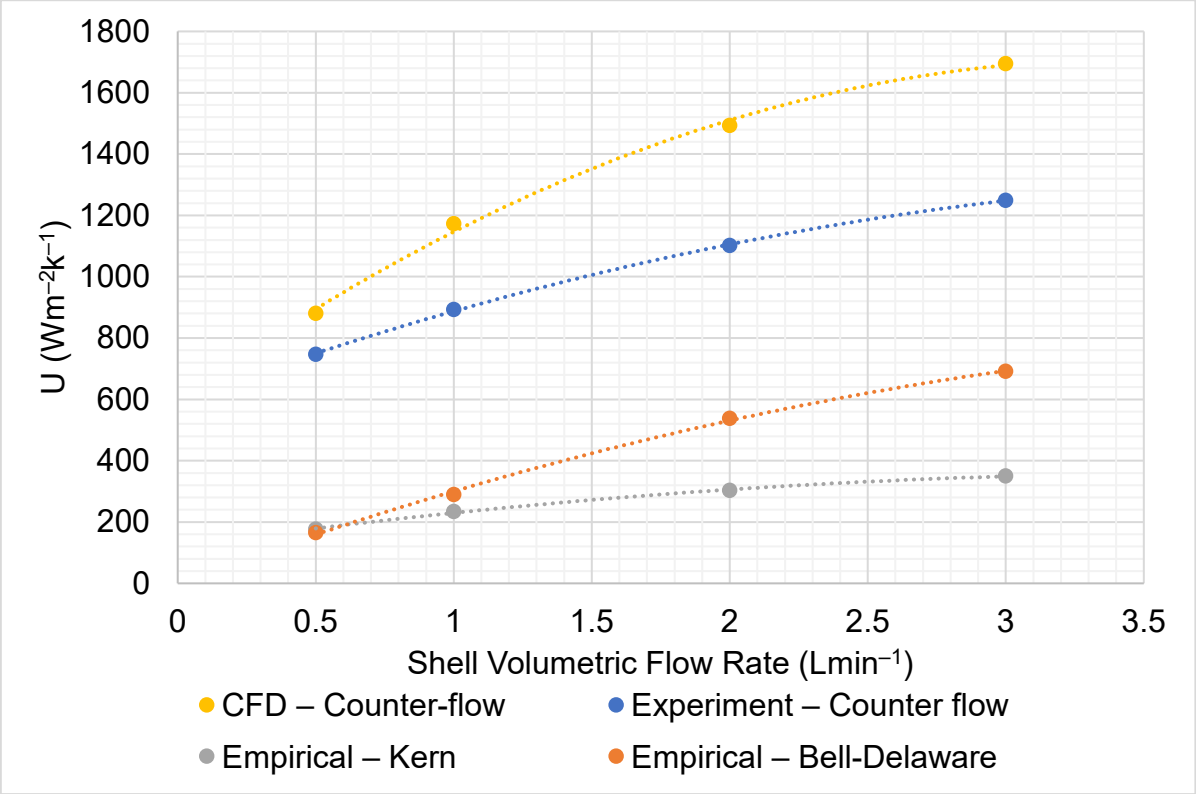

Figure 25: U vs. volumetric flow rate for the CFD, experimental, Bell-Delaware and Kern analyses – Counter-flow

Table 13: Counter-flow U results: CFD, UHX

Shell volumetric flow rate ($Lmin^{-1}$)	U ($Wm^{-2}K^{-1}$)		Percentage difference (%)
	Parallel	Counter	
0.5	838.80	880.83	5.01
1.0	1117.98	1172.75	4.90
2.0	1457.13	1493.10	2.47
3.0	1641.34	1694.80	3.26

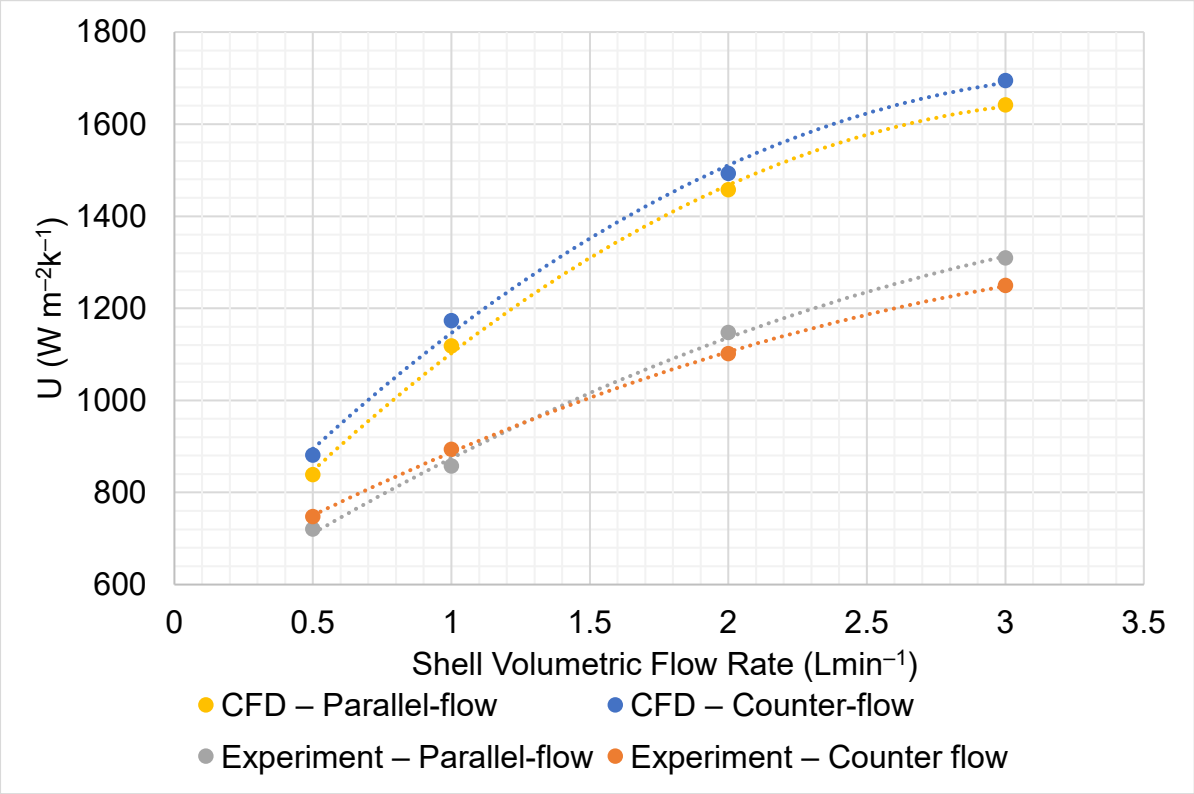

Figure 26: U vs. volumetric flow rate for both flow configurations

CFD model

When the CFD model was applied to the UHX geometry the results obtained were more accurate than the validation case. The decrease inlet flow rate meant that the average Y+ values for all the UHX simulations were below one with peak values below five. This increased with inlet flow rate but shows that for this model there was an increase in the boundary layer resolution allowing a greater utilisation of the SST turbulence model. The decrease in the quality of the boundary layer resolution for the higher volumetric flow rate simulations is resulting in greater inaccuracies. Mesh improvements are still needed in specific areas such as the outlet fillets and tubes below the inlet (Figure 27). Further, the increase in inaccuracies as flow rate increased suggest that the mesh independency study should have been carried out on the 2kgs^{-1} simulation instead of the 0.5kgs^{-1} simulation.

Using an adaptive timestep instead of a fixed timestep allowed an RMS residual target of 1x10^{-5} to be reached across all residuals. Transient effects were present in all cases though the temperature change was minimal. The standard deviation range for the tubes and shell outlet temperatures were 0.003-0.024K and 0.007-0.172K. The small deviations suggest that a converged solution has been reached within the five seconds simulated. However, it is still recommended that the simulations are run to five minutes, the time set out by the experiment, to allow a steady state solution to be reached. For the 0.5Lmin^{-1} case where the adaptive timestep was relatively large it meant that a settled oscillating solution was not reached. Where the timestep was smallest, for the 3Lmin^{-1} case, it resulted in an oscillating response. This further

suggests that the lower flow rate simulations should have been simulated for longer to allow the steady state solution to be reached.

Aside from mesh refinements the simulation setup can also be optimised. For example, transitional turbulence could be used to better represent the boundary layer and specifying an accurate turbulence intensity. Further, the geometry can be improved to better represent the UHX by introducing features such as baffles and manifolds.

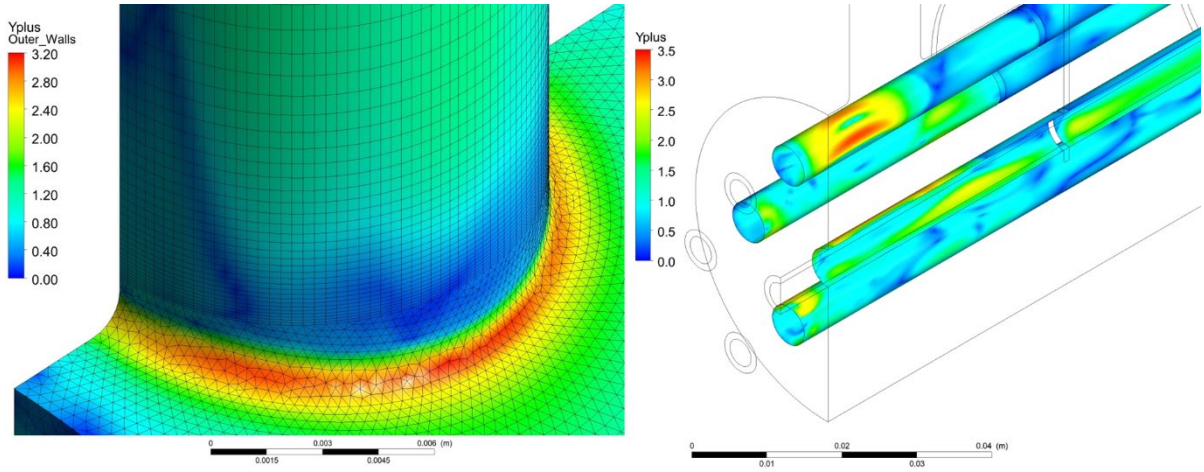

Figure 27: Location of higher Y+ values for the counter-flow 3Lmin^{-1} simulation

Conclusion

Initially the study by Ozden and Tari (2010) was used to validate the CFD method with a mesh sensitivity study and transient analysis also conducted. Next, this method was adapted for the UHX geometry where improvements from the validation case were applied. For the UHX two empirical methods were conducted which were also validated against data provided by Ozden and Tari (2010). These methods were then compared to an experimental analysis.

For the validation case the following conclusions were determined:

- The CFD techniques applied by Ozden and Tari (2010) do not represent the actual performance of the validation case heat exchanger
- This is primarily due to their poor mesh resolution and application of the k-ϵ turbulence model
- Hence, it is believed the actual values for U are 104–150% greater than theirs
- The CFD method developed here can be improved further with greater boundary layer mesh resolution and use of an adaptive timestep

For the university heat exchanger, it can be concluded:

- A more rigorous experimental method is needed to improve the accuracy of the results
- Leakage paths, fluctuations in inlet temperature and heat loss to the environment are also impacting the accuracy of the results
- Calculated results for the Kern and Bell-Delaware methods underpredicted the averaged experimental values by 73-76% and 46–77%
- The Kern and Bell-Delaware methods were not designed for the UHX geometry and therefore are not suitable for performance prediction
- The Bell-Delaware method was the more accurate method, but the baffle leakage correction factor was not included resulting in an overprediction of U
- The parallel-flow and counter-flow CFD results overpredicted the experimental results by 16-30% and 18-36%
- CFD results represent a geometrically perfect model and does not include any of the real-world problems present during the experimental analysis
- Therefore, the CFD analysis represents the closest results to the actual performance of the UHX and thus is the recommended analytical method
- The CFD model can be improved by applying specific mesh improvements, improvements to the setup and increasing the simulation time to five minutes

Overall, the three different analytical methods were applied to the UHX with the CFD analysis being the most suitable analytical method for predicting the performance of the UHX.

Future recommendations

The validation case CFD study should be revised to assess potential errors within the CFD method. Further, the model should be applied to other studies in the literature to assess the general suitability. A more rigorous experimental analysis should be carried out to assess the performance of the UHX. For example, the transient behaviour could be monitored using TECQUIPMENT's versatile data acquisition system. Further, the geometry of the heat exchanger could be improved to better represent the perfect nature of the CFD geometry and reduce the impact of the real-world problems.

A pressure drop analysis could also be carried out to provide a second comparison between the three analytical methods. The CFD method can be improved by running the simulations for a longer time with the aim to reach a steady state. Further, the modelling of manifolds to better predict the fluid entry into the tubes could improve the accuracy. Baffles could also be modelled to allow conduction to occur through

them. Furthermore, the CFD study can be used to assess possible modifications for the UHX to improve its performance characteristics.

Acknowledgements

I would like to extent my gratitude to my supervisor Adam Kyte for guidance and advice throughout the year. Secondly, I would like to thank Luke Lamplough and the virtual desktop team at the University of Plymouth.

Nomenclature

General

Symbol	Description	Unit
$U_{k,bd,e,c}$	Overall heat transfer coefficient (Kern, Bell-Delaware, experiment and CFD)	$Wm^{-2}K^{-1}$
$\dot{Q}$	Rate of heat transfer	W
A	Heat transfer area	m^2
$\Delta T_{ln,p,c,val}$	Log mean temperature difference (Parallel, counter-flow, validation)	K
C_p	Specific heat capacity at constant pressure	$(Jkg^{-1}K^{-1})$
ΔT	Temperature difference	K
ΔT_o	Temperature difference outlet	K
ΔT_i	Temperature difference inlet	K
T_{s1}	Shell inlet temperature	K
T_{s2}	Shell outlet temperature	K
T_{t2}	Tube outlet temperature	K
T_{t1}	Tube inlet temperature	K
T_w	Tube wall temperature	K
T_o	Shell outlet temperature	K
T_i	Shell inlet temperature	K
S_{tr}	Strouhal number	N/A
f_o	Oscillation frequency	s^{-1}
d_{to}	Tube outside diameter	m
u_a	Average shell velocity	ms^{-1}

Abbreviations

Abbreviation	Description
UHX	University heat exchanger
CFD	Computational fluid dynamics
SST	Shear stress transport
LMTD	Log mean temperature difference
RANS	Reynolds averaged Navier-stokes
RMS	Root mean squared
SD	Standard deviation

References

Ammar, S. M. & Park, C. W. (2020) 'Validation of the Gnielinski correlation for evaluation of heat transfer coefficient of enhanced tubes by non-linear regression model: An experimental study of absorption refrigeration system'. *International communications in heat and mass transfer*, 118 pp. 104819.

ANSYS (2011) 'ANSYS CFX-Solver Modeling Guide'.

ANSYS (2009) 'ANSYS CFX-Solver Theory Guide'. X`

ANSYS (2010) 'ANSYS Meshing User's Guide'.

Batalha Leoni, G., Suaiden Klein, T. & de Andrade Medronho, R. (2017) 'Assessment with computational fluid dynamics of the effects of baffle clearances on the shell side flow in a shell and tube heat exchanger'. *Applied thermal engineering*, 112 pp. 497-506.

Donald, K. (1950) *Process Heat Transfer.* New York: McGraw-Hill.

Eggenspieler, G. (2012) 'ANSYS CFX Turbulence modelling'.

El Maakoul, A., Laknizi, A., Saadeddine, S., El Metoui, M., Zaite, A., Meziane, M. & Ben Abdellah, A. (2016) 'Numerical comparison of shell-side performance for shell and tube heat exchangers with trefoil-hole, helical and segmental baffles'. *Applied thermal engineering*, 109 pp. 175-185.

Eryener, D. (2006) 'Thermoeconomic optimization of baffle spacing for shell and tube heat exchangers'. *Energy Conversion and Management*, 47 (11-12), pp. 1478-1489.

Holman, J. P. (2010) *Heat transfer*. 10th edn, international edn. Boston, Mass.: McGraw-Hill.

Katopodes, N. (2019) 'Viscous Fluid Flow'. Oxford, Cambridge: Butterworth-Heinemann.

Kays, W. M. and London, A. L. (1998) *Compact heat exchangers*. 3rd edn. Malabar, Fla.: Krieger Publications.

Levenspiel, O. (1984) *Engineering flow and heat exchange.* New York, London: Plenum.

Master, B. I., Chunangad, K. S. & Pushpanathan, V. (2003) 'Fouling Mitigation Using Helixchanger Heat Exchangers'. Menter, F. R. (2009) 'Review of the shear-stress transport turbulence model experience from an industrial perspective'. *International journal of computational fluid dynamics*, 23 (4), pp. 305-316.

Ozden E. *Detailed design of shell-and-tube heat exchangers using CFD. M.S. thesis, Middle East Technical University, Ankara, Turkey; 2007.*

Ozden, E. & Tari, I. (2010) 'Shell side CFD analysis of a small shell-and-tube heat exchanger'. *Energy Conversion and Management*, 51 (5), pp. 1004-1014.

Rogers, G. F. C. (1992) *Engineering thermodynamics : work and heat transfer.* ed. Mayhew, Y.R., 4th ed. edn. Harlow: Harlow : Longman.

Sayma, A. (2009) *Computational Fluid Dynamics. Bookboon.*

Schmidt-Nielsen, K. (1997) *Animal physiology : adaptation and environment.* 5th ed. edn. Cambridge: Cambridge University Press.

Taborek, J. & Spalding, B. (1983) 'Heat exchangers design handbook'.[in *Thermal and hydraulic design of heat exchnagers*. Hemisphere Publishing Corporation.

Tu, J., Yeoh, G. H. & Liu, C. (2007) *Computational Fluid Dynamics : A Practical Approach.* Burlington, UNITED KINGDOM: Elsevier Science & Technology.

Wang, Q., Chen, Q., Chen, G. & Zeng, M. (2009) 'Numerical investigation on combined multiple shell-pass shell-and-tube heat exchanger with continuous helical baffles'. *International journal of heat and mass transfer*, 52 (5), pp. 1214-1222.

Wen, J., Yang, H., Wang, S., Xue, Y. & Tong, X. (2015) 'Experimental investigation on performance comparison for shell-and-tube heat exchangers with different baffles'. *International journal of heat and mass transfer*, 84 pp. 990-997.

Appendices are provided separately as supplementary files (see additional downloads for this article).